# CHAPTER IV
# RESULTS AND DISCUSSION

## 4.1 Photocatalyst Characterizations

### 4.1.1 TG-DTG Results

The TG-DTG curves were used to study the thermal decomposition behavior of the synthesized dried photocatalysts and to obtain their suitable calcination temperature. Figures 4.1 and 4.2 show the TG-DTG curves of the dried pure $TiO_2$ and $0.95TiO_2$-$0.05ZrO_2$ mixed oxide gels, respectively. The DTG curves show three main exothermic regions. The details of all exothermic regions and their corresponding weight losses are summarized in Table 4.1. The first exothermic region, with its position lower than 150 °C, is attributed to the removal of physisorbed water molecules from the dried gels. The second exothermic region between 150 and 350 °C is attributed to the burnout of the surfactant molecules (Sreethawong *et al.*, 2009). The third exothermic region between 350 and 500 °C corresponds to the crystallization process of the photocatalysts and also the removal of organic remnants and chemisorbed water molecule (Hague *et al.*, 1994). The TG results reveal that the weight losses ended at a temperature of approximately 500 °C for both the dried photocatalysts. Therefore, the calcination temperature at 500 °C is sufficient for both the complete surfactant removal and the photocatalyst crystallization process. Therefore, the calcination temperature in the range of 500 and 900 °C was used to investigate its effect on the physicochemical properties and consequent photocatalytic hydrogen production activity.

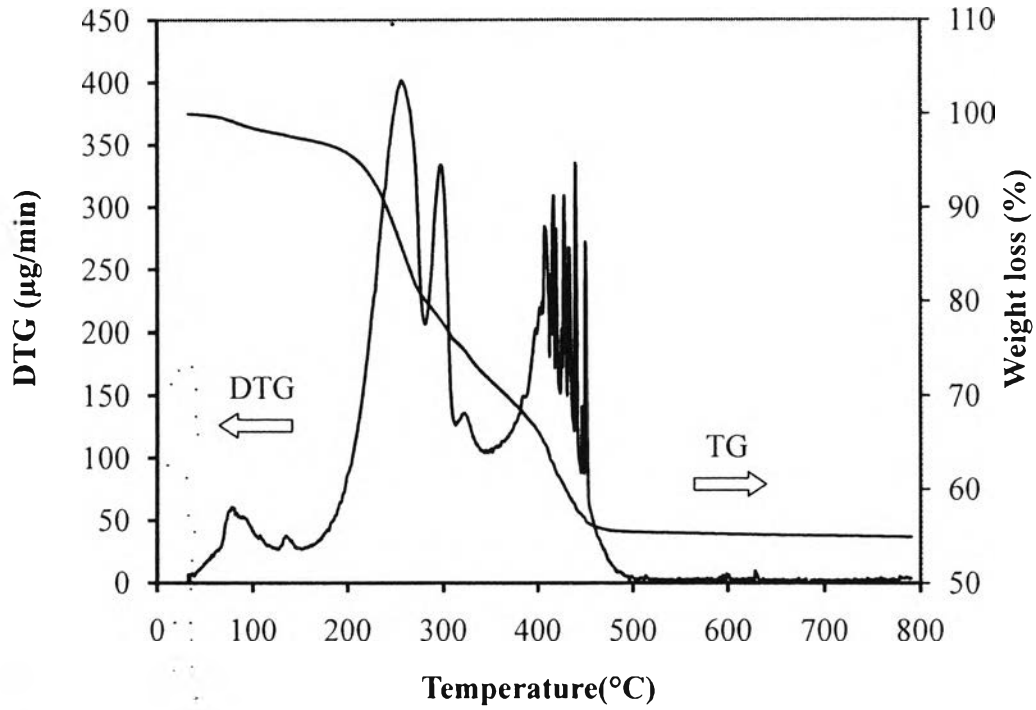


**Figure 4.1** TG-DTG curves of the dried synthesized pure $TiO_2$ photocatalyst.

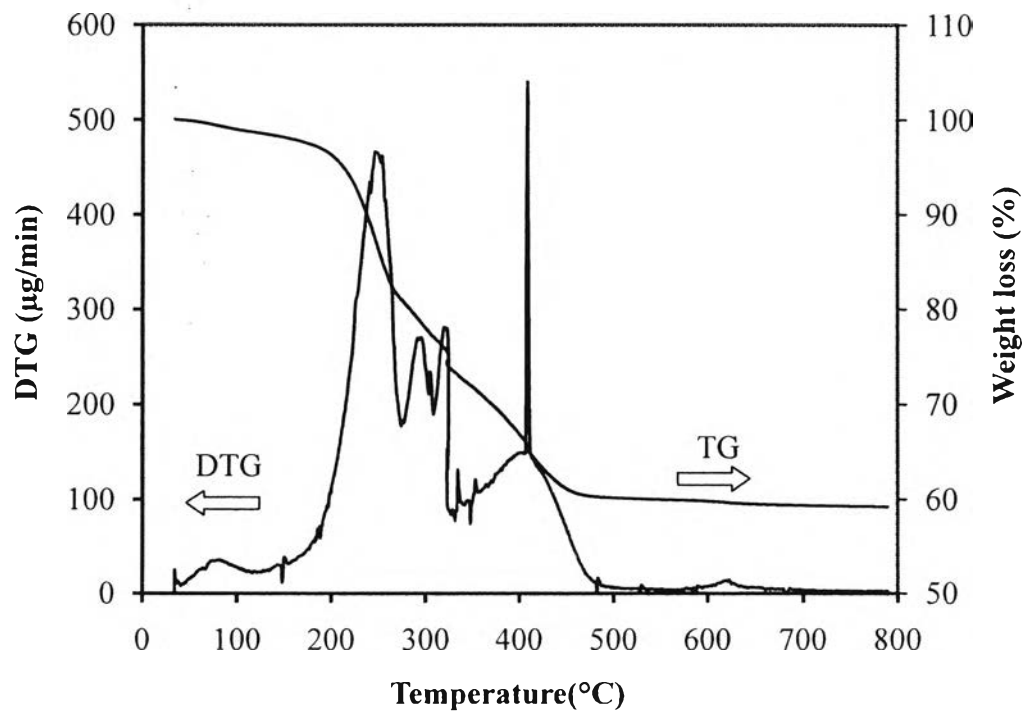


**Figure 4.2** TG-DTG curves of the dried synthesized $0.95TiO_2$-$0.05ZrO_2$ photocatalyst.

**Table 4.1** Thermal decomposition results of the dried synthesized pure $TiO_2$ and $0.95TiO_2$-$0.05ZrO_2$ mixed oxide photocatalysts from TG-DTG analysis

| Photocatalyst | Position of exothermic peak (°C) | | | | Corresponding weight loss (wt.%) | | | | |
|---|---|---|---|---|---|---|---|---|---|
| | 1st region | 2nd region | 3rd region | 4th region | 1st region | 2nd region | 3rd region | 4th region | Total |
| $TiO_2$ | 25-150 | 150-260 | 260-340 | 340-500 | 2.09 | 12.51 | 12.06 | 17.09 | 43.75 |
| $0.95TiO_2$-$0.05ZrO_2$ | 25-120 | 120-270 | 270-350 | 350-500 | 1.36 | 17.18 | 9.69 | 11.62 | 39.85 |

4.1.2 $N_2$ Adsorption-Desorption Results

The $N_2$ adsorption-desorption analysis was used to verify the mesoporosity of the $TiO_2$-$ZrO_2$ mixed oxide photocatalyst with different $TiO_2$-to-$ZrO_2$ molar ratios. The shape of the isotherms exhibits the characteristic behavior of the structure of powder, which is composed of an assembly of particles with large open packing. The adsorption-desorption isotherms of the pure $TiO_2$ calcined at 500 °C for 4 h, the $0.95TiO_2$-$0.05ZrO_2$ mixed oxide calcined at 800 °C for 4 h, and the 0.5 wt.% Pt-loaded $0.95TiO_2$-$0.05ZrO_2$ mixed oxides calcined at 800 °C are shown in Figures 4.3, 4.4 and 4.5, respectively. All of the samples exhibited a typical IUPAC type IV pattern with an H2-type hysteresis loop, which is the characteristic of a mesoporous-assembled material (mesoporous size between 2 and 50 nm) according to the classification of IUPAC (Rouquerol *et al.*, 1999). A sharp increase in the adsorption curves at a high relative pressure ($P/P_0$) implies a capillary condensation of $N_2$ molecules inside the mesopores, implying the well-uniform mesopores and narrow pore size distribution since the relative pressure position of the inflection point is directly related to the pore dimension. The insets of Figures 4.3, 4.4 and 4.5 show pore size distributions calculated from the desorption branch of the isotherms by the DH method. The pure mesoporous-assembled $TiO_2$ and $0.95TiO_2$-$0.05ZrO_2$ mixed oxides without and with 0.5 wt.% Pt loading possessed quite narrow pore size distributions entirely locating in the mesopore region, implying a good quality of the samples. However, it was experimentally found that the mixed oxides with $TiO_2$-to-

$ZrO_2$ molar ratios ranging from 60:40 to 20:80, as well as the pure $ZrO_2$, exhibited a typical IUPAC type II pattern, indicating that the samples mainly contained macropores (macroporous size greater than 50 nm) (Rouquerol *et al.*, 1999). This can be explained by the amorphous-nature structure of the $ZrO_2$ with relatively high contents (Schattka *et al.*, 2002), which contributed to the macroporous characteristic.

Table 4.2 shows the textural properties obtained from the $N_2$ adsorption-desorption analysis of $TiO_2$-$ZrO_2$ mixed oxide photocatalysts with different $TiO_2$-to-$ZrO_2$ molar ratios. It is clearly observed that the addition of $ZrO_2$ resulted in an increase in specific area, as can be seen from the results that by incorporating 5 mol% $ZrO_2$ in the pure $TiO_2$, the surface area increased from 61.7 to 116.1 $m^2 \cdot g^{-1}$ at a calcination temperature of 500 °C. This is because the presence of this second metal oxide with sufficient amounts can retard crystallization process and affect the growth of bulk material (Reddy *et al.*, 1992), which was confirmed by using the XRD analysis in the next section, resulting in higher surface areas of the mixed oxide photocatalysts. In case of increasing calcination temperature from 500 to 900 °C, it can be seen from Table 4.2 that the 5 mol% $ZrO_2$-modified $TiO_2$ ($0.95TiO_2$-$0.05ZrO_2$), which possessed a larger surface area at a low temperature (500 °C), can retain its surface area rather than the pure $TiO_2$ at higher temperatures. The surface area of the pure $TiO_2$ was smaller and decreased more quickly from 61.7 to 2.2 $m^2 \cdot g^{-1}$ as compared to the $0.95TiO_2$-$0.05ZrO_2$ mixed oxide, of which the surface area decreased from 116.1 to 17.7 $m^2 \cdot g^{-1}$. The observed loss in the surface area with increasing calcination temperature is because of the pore coalescence due to the crystallization of walls separating the mesopores. This tendency also caused an increase in the mean mesopore diameter and a decrease in the total pore volume of the materials. For the effect of calcination time on the texural properties of the $0.95TiO_2$-$0.05ZrO_2$ mixed oxide at a given calcination temperature of 500 °C, the surface area, mean mesopore diameter, and total pore volume only changed slightly with increasing calcination time from 2 and 8 h, indicating a superior impact of the calcination temperature on the texural propertied to the calcination time.

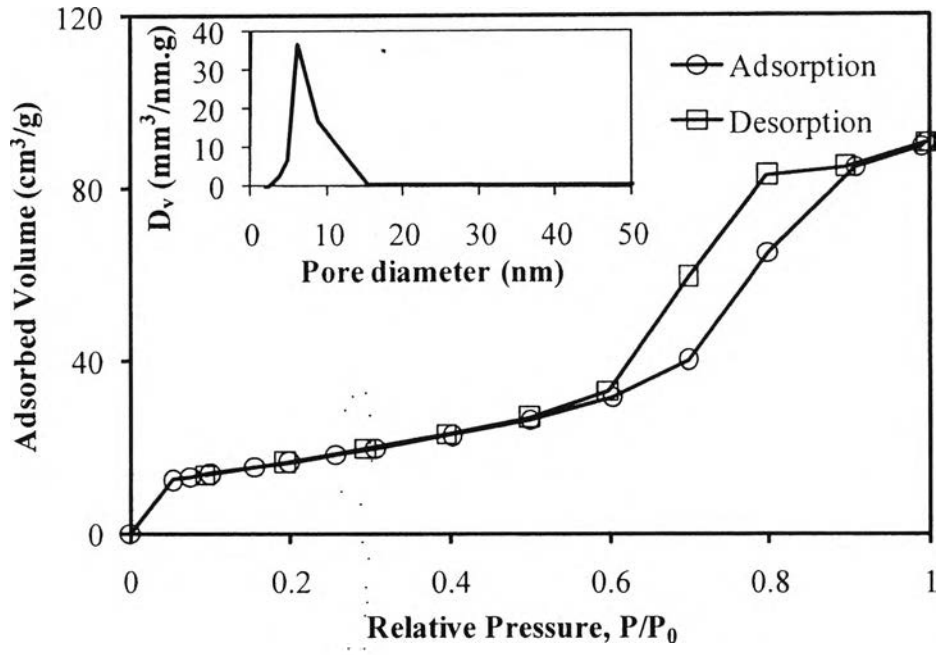


**Figure 4.3** $N_2$ adsorption-desorption isotherms and pore size distribution of the synthesized pure $TiO_2$ calcined at 500 °C for 4 h (Inset: pore size distribution).

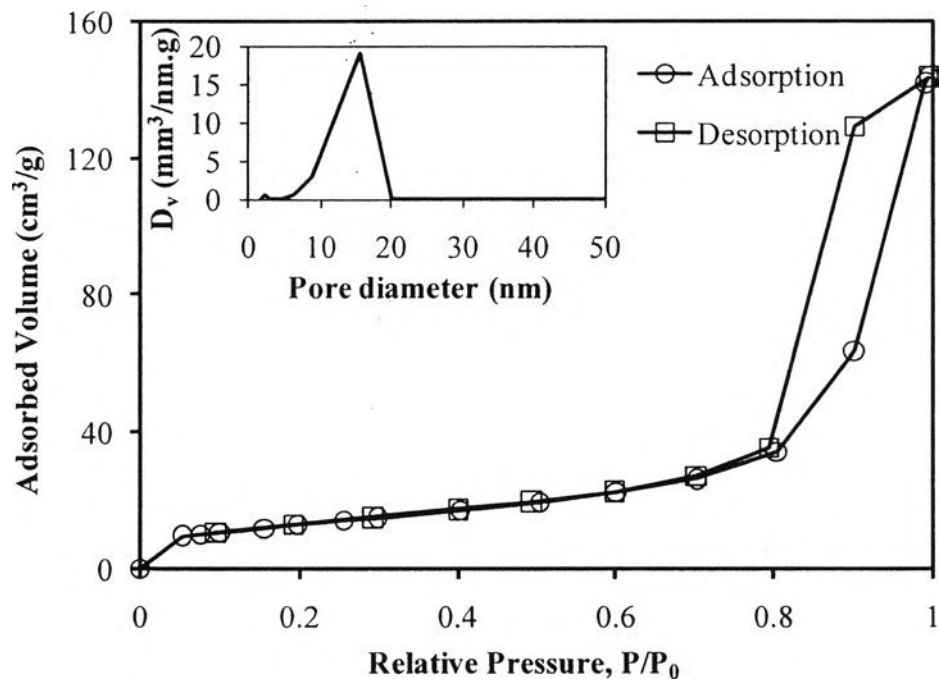


**Figure 4.4** $N_2$ adsorption-desorption isotherms and pore size distribution of the synthesized $0.95TiO_2$-$0.05ZrO_2$ mixed oxide calcined at 800 °C for 4 h (Inset: pore size distribution).

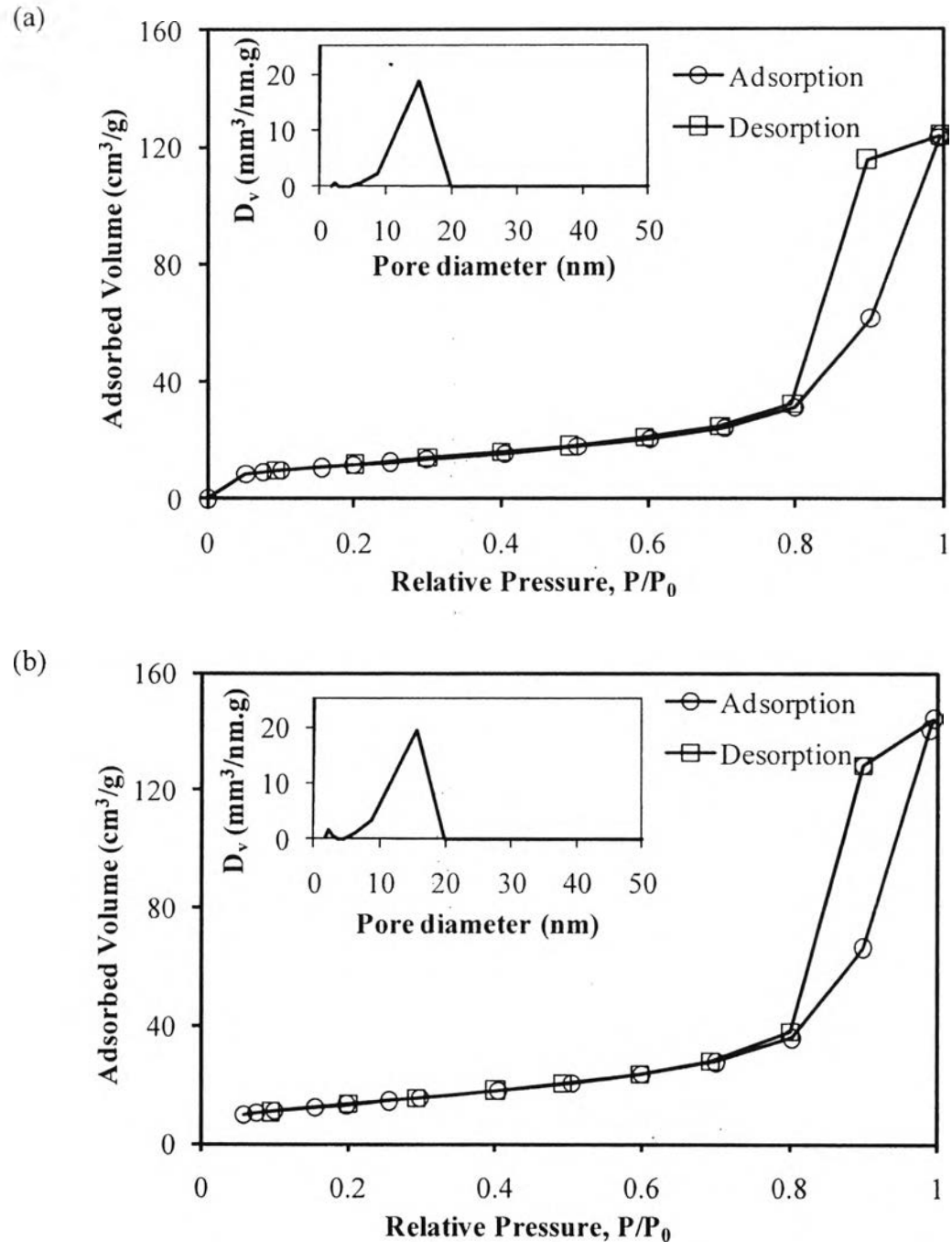


**Figure 4.5** $N_2$ adsorption-desorption isotherms and pore size distributions of the synthesized 0.5 wt.% Pt-loaded $0.95TiO_2$-$0.05ZrO_2$ mixed oxide calcined at 800 °C for 4 h and prepared by (a) SSSG method and (b) PCD method (Inset: pore size distribution).

**Table 4.2** Summary of $N_2$ adsorption-desorption results of the synthesized mesoporous-assembled $TiO_2$-$ZrO_2$ mixed oxide photocatalysts

| Photocatalyst | Calcination temperature (°C) | Calcination time (h) | BET surface area ($m^2 \cdot g^{-1}$) | Mean mesopore diameter (nm) | Total pore volume ($cm^3 \cdot g^{-1}$) |
|---|---|---|---|---|---|
| $TiO_2$ | 500 | 4 | 61.7 | 6.12 | 0.138 |
| | 600 | | 18.4 | 6.09 | 0.049 |
| | 700 | | 3.2 | -[a] | -[a] |
| | 800 | | 3.5 | -[a] | -[a] |
| | 900 | | 2.2 | -[a] | -[a] |
| $0.95TiO_2$-$0.05ZrO_2$ | 500 | 2 | 131.7 | 6.14 | 0.253 |
| | | 4 | 122.1 | 6.17 | 0.241 |
| | | 6 | 124.0 | 6.17 | 0.250 |
| | | 8 | 124.9 | 6.16 | 0.256 |
| | 600 | 4 | 86.7 | 8.79 | 0.198 |
| | 700 | | 79.2 | 8.87 | 0.239 |
| | 800 | | 47.2 | 15.65 | 0.220 |
| | 900 | | 17.7 | -[a] | -[a] |
| $0.8TiO_2$-$0.2ZrO_2$ | 500 | 4 | 90.9 | 8.81 | 0.291 |
| $0.6TiO_2$-$0.4ZrO_2$ | | | 189.9 | -[a] | -[a] |
| $0.4TiO_2$-$0.6ZrO_2$ | | | 189.2 | -[a] | -[a] |
| $0.2TiO_2$-$0.8ZrO_2$ | | | 133.0 | -[a] | -[a] |
| $ZrO_2$ | | | 31.3 | -[a] | -[a] |

[a] $N_2$ adsorption-desorption isotherms corresponded to an IUPAC type II pattern.

Table 4.3 shows the summary of textural properties obtained from the $N_2$ adsorption-desorption isotherms of the Pt-loaded mesoporous-assembled $0.95TiO_2$-$0.05ZrO_2$ mixed oxide photocatalysts calcined at 800 °C and prepared by the single-step sol-gel (SSSG) and photochemical deposition (PCD) methods with various Pt loadings. The results showed that the surface area of the Pt-loaded $0.95TiO_2$-$0.05ZrO_2$ mixed oxides prepared by the SSSG method slightly decreased with increasing Pt loading, while the mean mesopore diameter and total pore volume remained almost the same as those of the $0.95TiO_2$-$0.05ZrO_2$ mixed oxide support. The slight decrease in the surface area when the Pt particles were deposited on the support by the SSSG method can be possibly attributed to the blockage of a small portion of mesopores of the support by the Pt particles buried inside the mesoporous-assembled structure. In contrast, for the Pt-loaded $0.95TiO_2$-$0.05ZrO_2$ mixed oxides prepared by the PCD method, the Pt particles deposited mainly on the outer surface of the photocatalyst support. The surface area of these deposited Pt particles may contribute to a slightly higher surface area as compared to the unloaded $0.95TiO_2$-$0.05ZrO_2$ mixed oxide, while the mean mesopore diameter and total pore volume remained almost unchanged at various Pt loadings. However, there was no significant difference in the surface areas observed for the Pt-loaded samples prepared by both the SSSG and PCD methods, possibly because of the very low Pt loadings.

Table 4.4 shows the summary of textural properties obtained from the $N_2$ adsorption-desorption isotherms of the 0.5 wt.% Pt-loaded mesoporous-assembled $0.95TiO_2$-$0.05ZrO_2$ mixed oxide photocatalysts calcined at 800 °C and prepared by the PCD method under various conditions. The results showed that the UV light irradiation time of 2 h and UV light intensity of 44 W gave the highest surface area of the Pt-loaded mixed oxide photocatalyst at about 49.4 $m^2 \cdot g^{-1}$. However, there were no significant differences in the surface area, as well as the mean mesopore diameter and total pore volume, by varying both UV light irradiation time and UV light intensity.

**Table 4.3** Summary of $N_2$ adsorption-desorption results of the synthesized Pt-loaded mesoporous-assembled $0.95TiO_2$-$0.05ZrO_2$ mixed oxide photocatalysts calcined at 800 °C for 4 h and prepared by SSSG and PCD methods

| Preparation method | Pt loading (wt.%) | BET surface area ($m^2 \cdot g^{-1}$) | Mean mesopore diameter (nm) | Total pore volume ($cm^3 \cdot g^{-1}$) |
|---|---|---|---|---|
| SSSG | - | 47.2 | 15.65 | 0.220 |
| | 0.3 | 43.4 | 15.46 | 0.181 |
| | 0.5 | 42.5 | 15.14 | 0.190 |
| | 0.7 | 42.7 | 15.56 | 0.200 |
| | 1 | 42.3 | 15.69 | 0.196 |
| PCD[a] | - | 47.2 | 15.65 | 0.220 |
| | 0.3 | 47.6 | 15.50 | 0.218 |
| | 0.5 | 49.4 | 15.64 | 0.218 |
| | 0.7 | 48.5 | 15.32 | 0.221 |
| | 1 | 48.2 | 15.67 | 0.219 |

[(a)] Prepared with UV light irradiation time of 2 h and UV light intensity of 44 W

**Table 4.4** Summary of $N_2$ adsorption-desorption results of the synthesized 0.5 wt.% Pt-loaded mesoporous-assembled $0.95TiO_2$-$0.05ZrO_2$ mixed oxide photocatalysts calcined at 800 °C for 4 h and prepared by PCD method under various conditions

| PCD conditions | | BET surface area ($m^2 \cdot g^{-1}$) | Mean mesopore diameter (nm) | Total pore volume ($cm^3 \cdot g^{-1}$) |
|---|---|---|---|---|
| UV light source intensity (W) | UV light irradiation time (h) | | | |
| 44 | 1 | 49.2 | 15.51 | 0.213 |
| | 2 | 49.4 | 15.64 | 0.218 |
| | 3 | 48.1 | 15.49 | 0.217 |
| 22 | 2 | 47.1 | 15.65 | 0.211 |
| 44 | | 49.4 | 15.64 | 0.218 |
| 88 | | 48.1 | 15.74 | 0.216 |

4.1.3 XRD Results

The XRD patterns of the mesoporous-assembled $TiO_2$-$ZrO_2$ mixed oxide photocatalysts with different $TiO_2$-to-$ZrO_2$ molar ratios and calcined at 500 °C for 4 h are shown in Figure 4.6. The XRD pattern of the pure $TiO_2$ showed a crystalline structure of the pure anatase phase with the dominant peaks at 2θ of about 25.2, 37.9, 48.3, 53.8, 62.7, 68.9, and 75.3°, which represent the indices of (101), (103), (200), (105), (213), (116), and (107) planes of the anatase $TiO_2$, respectively (Smith, 1960). The $TiO_2$-$ZrO_2$ mixed oxide samples with $TiO_2$-to-$ZrO_2$ molar ratios of 95:5, 80:20, and 60:40 also showed diffraction peaks attributed to the anatase $TiO_2$. However, the peak intensities decreased with increasing $ZrO_2$ content possibly because a higher $ZrO_2$ content retarded the crystallization process of the $TiO_2$. No clear crystallinity was observed in the $TiO_2$-$ZrO_2$ mixed oxides with $ZrO_2$ contents of 60 and 80%, implying that these high $ZrO_2$ contents had an extremely strong capability of retarding the crystallization due to their homogeneous distribution in the

bulk material (Wang *et al.*, 2006). For the pure $ZrO_2$, the XRD pattern exhibits only a tetragonal phase structure with.dominant peaks at 2θ of about 30 and 35°, which represent the index of (111) and (200) planes of the tetragonal $ZrO_2$, respectively (Zhang *et al.*, 2008).

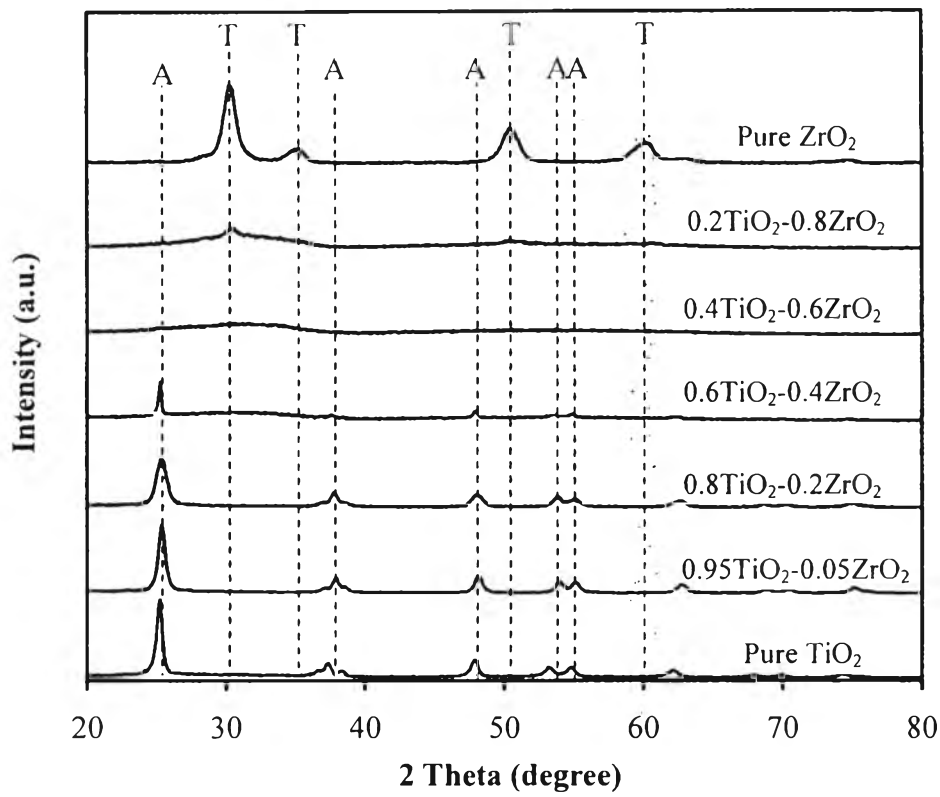


**Figure 4.6** XRD patterns of the mesoporous-assembled $TiO_2$-$ZrO_2$ mixed oxide photocatalysts calcined at 500 °C for 4 h (A = Anatase $TiO_2$, T = Tetragonal $ZrO_2$).

Figure 4.7 shows the XRD patterns of the pure $TiO_2$ and $0.95TiO_2$-$0.05ZrO_2$ mixed oxide photocatalysts calcined a various temperatures. From Figure 4.7(a), the XRD pattern of the pure $TiO_2$ calcined at 500 °C showed a crystalline structure of the pure anatase phase, as mentioned above. The pure $TiO_2$ underwent the anatase-to-rutile phase transformation beginning at 600 °C, resulting in the combination of the anatase and rutile phases. The occurrence of the dominant peaks at 2θ of about 27.5, 36.0, 41.2, 44.1, 54.2, 56.7, and 64.2°, which correspond to the indices of (110), (101), (111), (210), (211), (220), (310), and (301) planes, respectively, indicated the presence of the rutile $TiO_2$. The rutile ratio ($W_R$) in terms

of its weight fraction was estimated from the XRD intensity data by using Eq. (4.1) (Spurr and Myers, 1957):

$$W_R = [1 + 0.8I_A/I_R]^{-1} \quad (4.1)$$

where $I_A$ and $I_R$ represent the integrated intensities of anatase (101) and rutile (110) diffraction peaks, respectively. All calculated values of the rutile ratio ($W_R$) are presented in Table 4.5. A steadily increased transformation was observed until the photocatalyst contained only the pure rutile phase after calcined at 900 °C. However, this phase transformation behavior did not occur for the $0.95TiO_2$-$0.05ZrO_2$ mixed oxide. Figure 4.7(b) shows that the addition of 5 mol% $ZrO_2$ delayed the phase transformation of $TiO_2$ from the meta-stable anatase phase to the thermally stable rutile phase (Lin *et al.*, 1994), since the $0.95TiO_2$-$0.05ZrO_2$ mixed oxide exhibited the only dominant XRD peaks corresponding to the pure anatase phase even when it was calcined at 800 °C. In case of varying calcination time, the photocatalysts calcined at 500 °C for 2 to 8 h exhibited no significant difference in the intensity of the anatase peaks (Figure 4.8), as shown later by the similar crystallite size. The results indicated that the crystallite size growth with respect to the calcination time was slow at a given calcination temperature of 500 °C.

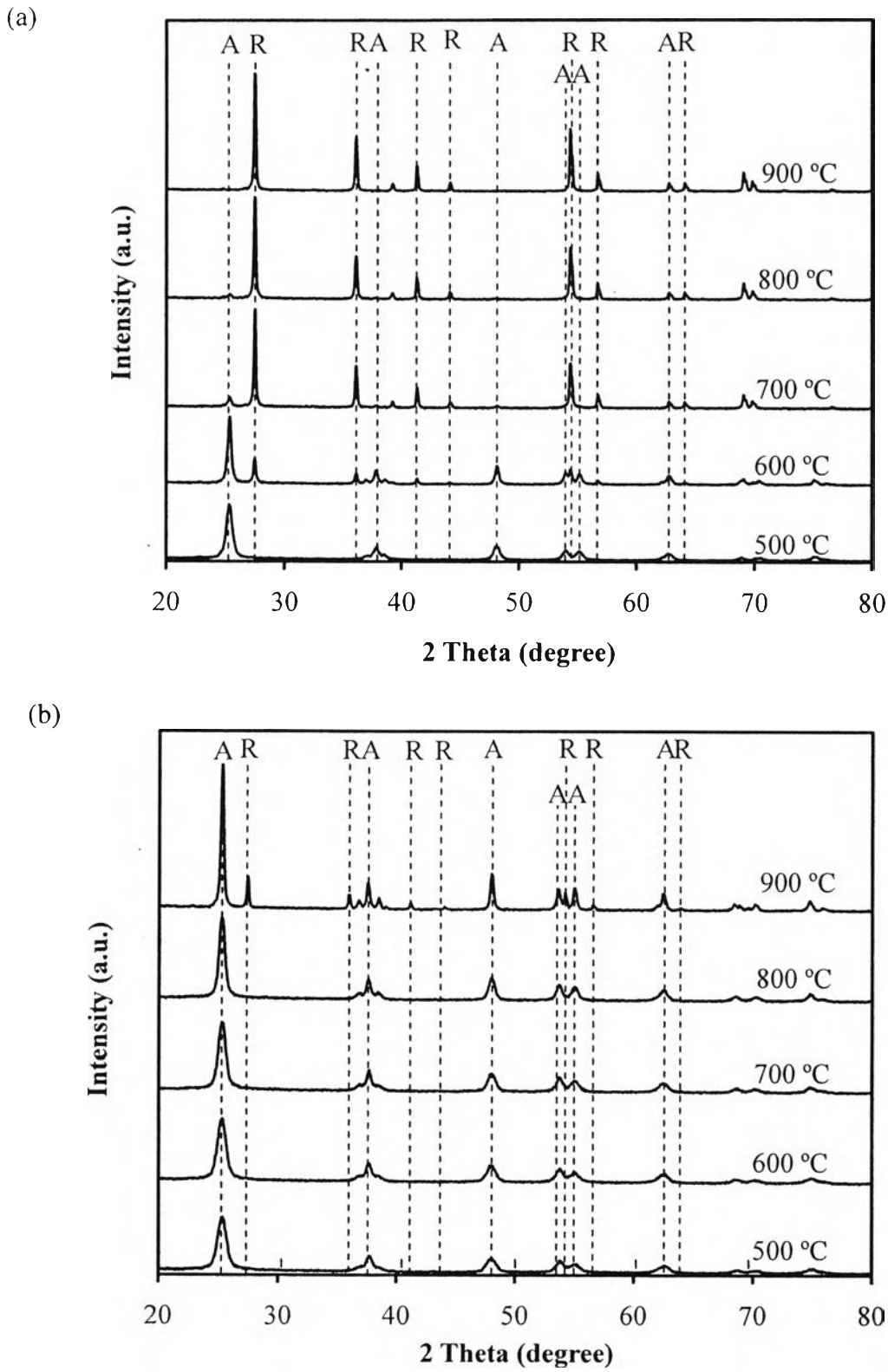


**Figure 4.7** XRD patterns of the mesoporous-assembled (a) $TiO_2$ and (b) $0.95TiO_2$-$0.05ZrO_2$ mixed oxide photocatalysts calcined at various temperatures for 4 h (A = Anatase $TiO_2$, R = Rutile $TiO_2$).

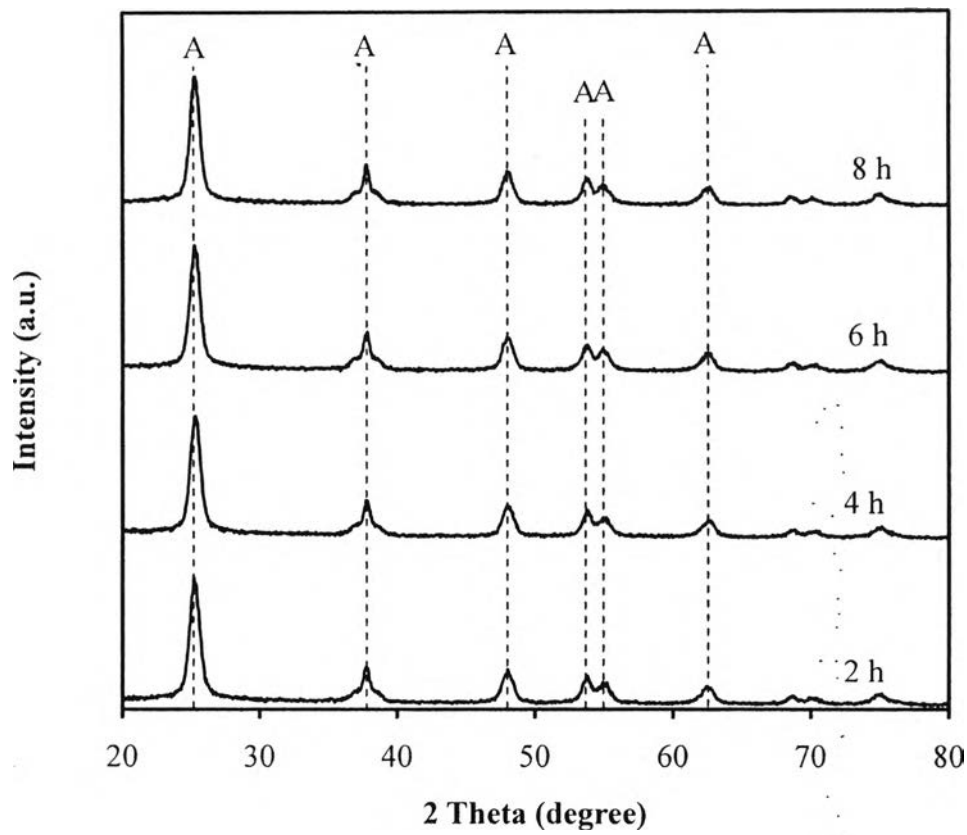


**Figure 4.8** XRD patterns of the mesoporous-assembled $0.95TiO_2$-$0.05ZrO_2$ mixed oxide photocatalysts calcined at 500 °C at various calcination time (A = Anatase $TiO_2$).

**Table 4.5** Summary of XRD results of the synthesized mesoporous-assembled $TiO_2$-$ZrO_2$ mixed oxide photocatalysts

| Photocatalyst | Calcination temperature (°C) | Calcination time (h) | Phase from XRD pattern | Rutile ratio, $W_R$ | Crystallite size (nm) | |
|---|---|---|---|---|---|---|
| | | | | | Anatase (101) | Rutile (110) |
| $TiO_2$ | 500 | 4 | Anatase | - | 13.70 | - |
| | 600 | | Anatase + Rutile | 0.29 | 15.23 | 15.30 |
| | 700 | | Anatase + Rutile | 0.92 | - | 15.30 |
| | 800 | | Anatase + Rutile | 0.97 | - | 17.18 |
| | 900 | | Rutile | 1.00 | - | 17.18 |
| $0.95TiO_2$-$0.05ZrO_2$ | 500 | 2 | Anatase | - | 10.53 | - |
| | | 4 | Anatase | - | 9.14 | - |
| | | 6 | Anatase | - | 9.78 | - |
| | | 8 | Anatase | - | 9.78 | - |
| | 600 | 4 | Anatase | - | 9.13 | - |
| | 700 | | Anatase | - | 10.53 | - |
| | 800 | | Anatase | - | 12.45 | - |
| | 900 | | Anatase + Rutile | 0.19 | 15.23 | 17.18 |
| $0.8TiO_2$-$0.2ZrO_2$ | 500 | 4 | Anatase | - | 8.71 | - |
| $0.6TiO_2$-$0.4ZrO_2$ | | | Anatase | - | 7.16 | - |
| $0.4TiO_2$-$0.6ZrO_2$ | | | Amorphous | - | - | - |
| $0.2TiO_2$-$0.8ZrO_2$ | | | Amorphous | - | - | - |
| $ZrO_2$[a] | | | Tetragonal | - | - | - |

[(a)] Crystallite size of $ZrO_2$ determined from the tetragonal (111) peak at 2θ of 30° = 9.23 nm.

The XRD patterns of the Pt-loaded $0.95TiO_2$-$0.05ZrO_2$ mixed oxides calcined at 800 °C and prepared by the SSSG and PCD methods are shown in Figure 4.9. All the diffraction peaks corresponded to the crystalline structure of the anatase $TiO_2$. The presence of Pt in the photocatalysts prepared by both methods could be observed at high Pt loadings by a diffraction peak at 2θ of 39.8°, which corresponds to the index of Pt (111) plane; however, the peak intensity was quite weak possibly because of its low content and high dispersion.

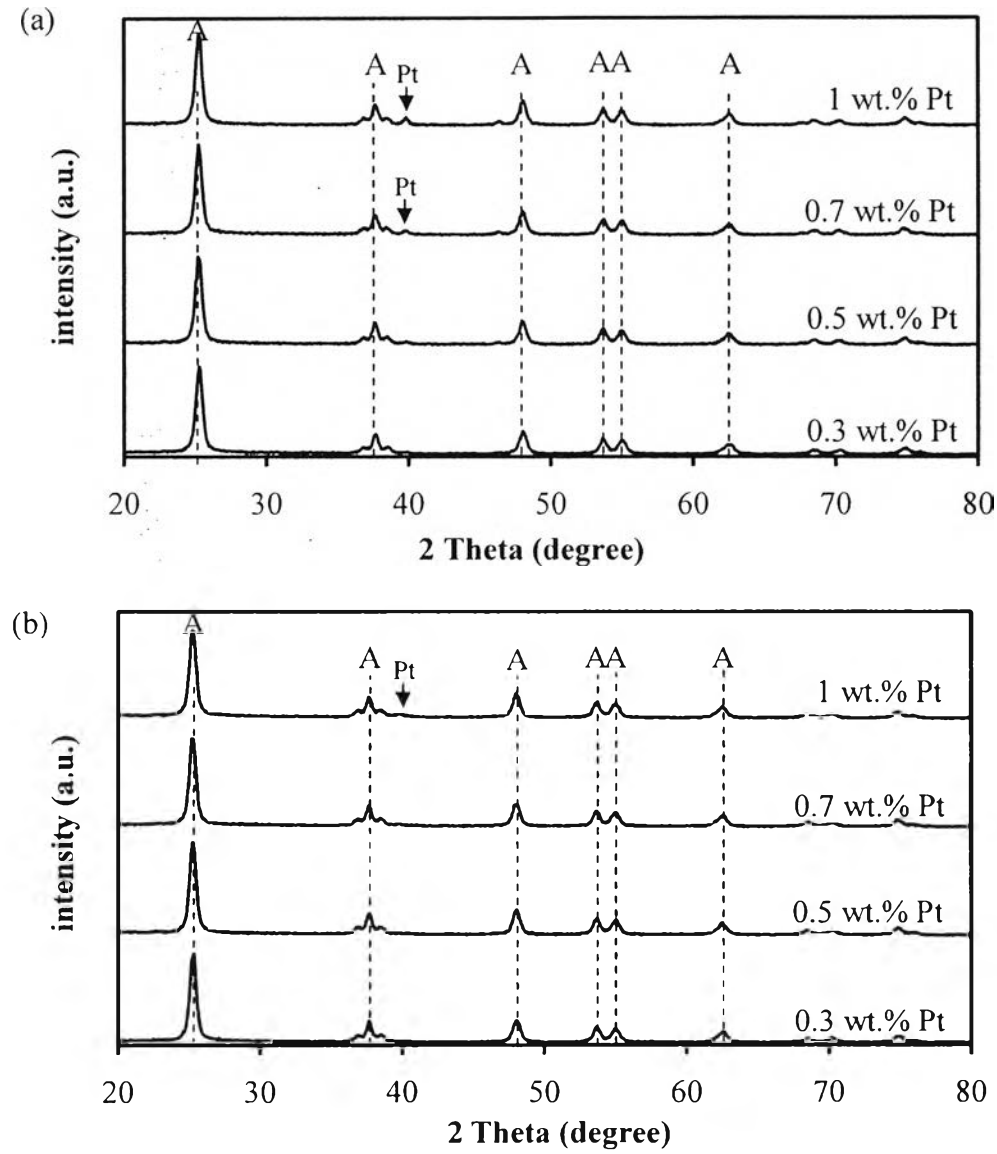


**Figure 4.9** XRD patterns of the Pt-loaded mesoporous-assembled $0.95TiO_2$-$0.05ZrO_2$ mixed oxide photocatalysts with various Pt loadings calcined at 800 °C and prepared by (a) SSSG and (b) PCD methods (A = Anatase $TiO_2$).

Figures 4.10 and 4.11 show the XRD patterns of the 0.5 wt.% Pt-loaded $0.95TiO_2$-$0.05ZrO_2$ mixed oxide photocatalysts calcined at 800 °C and prepared by the PCD method under various UV light irradiation times and UV light intensities, respectively. The result showed that all of the diffraction peaks were in the crystalline structure of the anatase $TiO_2$, and there were no significant differences in the intensity of the anatase peaks by varying both UV light irradiation time and UV light intensity. In addition, the Pt diffraction peaks were not clearly observed due to the low Pt loading, as mention above.

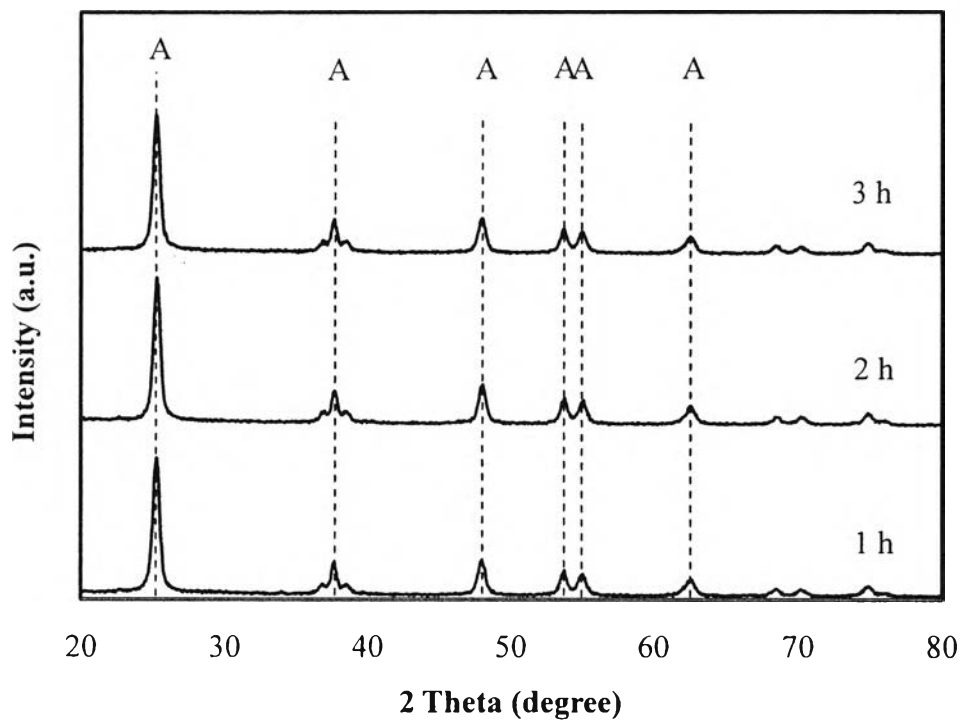


**Figure 4.10** XRD patterns of the 0.5 wt.% Pt-loaded mesoporous-assembled $0.95TiO_2$-$0.05ZrO_2$ mixed oxide photocatalysts calcined at 800 °C and prepared by PCD method under various UV light irradiation times at the UV light intensity of 44 W (A = Anatase $TiO_2$).

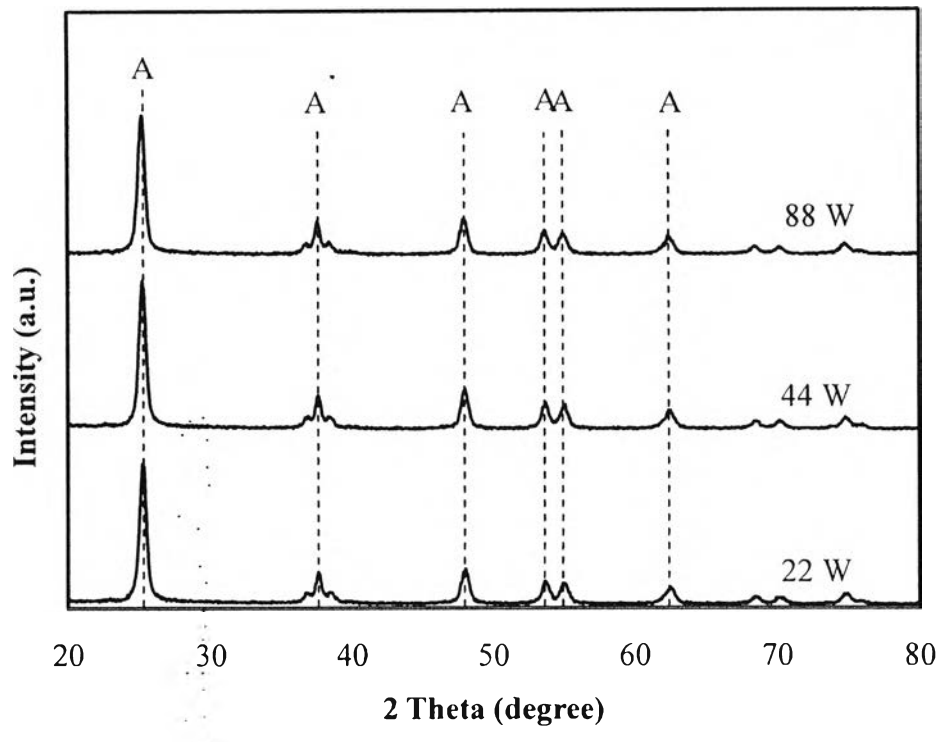


**Figure 4.11** XRD patterns of the 0.5 wt.% Pt-loaded mesoporous-assembled $0.95TiO_2$-$0.05ZrO_2$ mixed oxide photocatalysts calcined at 800 °C and prepared by PCD method under various UV light intensities at the UV light irradiation time of 2 h (A = Anatase $TiO_2$)

The crystallite size of the photocatalysts was calculated from the line broadening of the most preferentially oriented diffraction peak of each crystalline phase according to the Sherrer equation (Cullity, 1978) (Eq. 4.2):

$$L = \frac{k\lambda}{\beta\cos(\theta)} \tag{4.2}$$

where L is the crystallite size, k is the Sherrer constant usually taken as 0.89, $\lambda$ is the wavelength of the X-ray radiation (0.15418 nm for Cu K$\alpha$), $\beta$ is the full width at half maximum (FWHM) of the diffraction peak measured at $2\theta$, and $\theta$ is the diffraction angle. The crystallite sizes of all the synthesized photocatalysts are given in Tables 4.5 and 4.6. The results revealed that the addition of $ZrO_2$ led to the decrease in crystallite size due to the role of $ZrO_2$ in retarding the growth of the crystals, as mentioned above. With increasing calcination temperature, a larger crystallite size was observed for both pure $TiO_2$ and $0.95TiO_2$-$0.05ZrO_2$ mixed oxide photocatalysts

due to the grain growth induced by an increased temperature. However, the calcination time insignificantly affected the crystallite size of the $0.95TiO_2$-$0.05ZrO_2$ mixed oxide, as previously shown by almost the same intensity of the anatase peaks. For the Pt-loaded $0.95TiO_2$-$0.05ZrO_2$ mixed oxide photocatalysts prepared by both the SSSG and PCD methods, the crystallite size was in average slightly larger than that of the unloaded $0.95TiO_2$-$0.05ZrO_2$ mixed oxide at the same calcination temperature, while the Pt loading insignificantly affected the crystallite size possibly due to its relatively low content.

**Table 4.6** Summary of XRD results of the synthesized Pt-loaded mesoporous-assembled $0.95TiO_2$-$0.05ZrO_2$ mixed oxide photocatalysts calcined at 800 °C for 4 h and prepared by SSSG and PCD methods

| Preparation method | Pt loading (wt.%) | Phase from XRD pattern | Anatase (101) crystallite size (nm) |
|---|---|---|---|
| SSSG | 0.3-1 | Anatase | 15.23 |
| PCD[a] | 0.3-1 | Anatase | 15.23 |

[a] Prepared with UV light irradiation time of 2 h and UV light intensity of 44 W

4.1.4 UV-Visible Spectroscopy Results

UV-visible spectroscopy was used to examine the light absorption ability of the synthesized mesoporous-assembled $TiO_2$-$ZrO_2$ mixed oxide photocatalysts without and with Pt loading, as well as that of Eosin Y (E.Y.) solution, which was used as a sensitizer for the photocatalytic $H_2$ production in this work. Figure 4.12 shows the UV-visible spectra of the mesoporous-assembled $TiO_2$-$ZrO_2$ mixed oxide photocatalysts with different $TiO_2$-to-$ZrO_2$ molar ratios calcined at 500 °C. The results of absorption onset wavelength and corresponding band gap energy of all the photocatalysts obtained from the UV-visible spectra are summarized

in Table 4.7. It is clearly seen that the absorption bands of the synthesized mesoporous-assembled $TiO_2$-$ZrO_2$ mixed oxide photocatalysts were mainly in the UV light region of 200 to 400 nm. The band gap energy ($E_g$, eV) was determined by extrapolating the onset of the rising part to x-axis ($\lambda_g$, nm) of the plots, as shown by dashed line in Figure 4.12, and calculated by Eq. (4.3):

$$E_g = 1240 / \lambda_g \tag{4.3}$$

where $\lambda_g$ is the wavelength (nm) of the exciting light. With increasing $ZrO_2$ content in the mixed oxide photocatalysts, the band gap energy gradually increased from 3.22 ($\lambda_g$ = 385 nm) for the pure $TiO_2$ to 3.37 eV ($\lambda_g$ = 368 nm) for the $0.2TiO_2$-$0.8ZrO_2$ mixed oxide. The shift of the absorption onset edge in the $TiO_2$-$ZrO_2$ mixed oxides can be attributed to quantum-size effect for smaller crystallites (Andrulevicius *et al.*, 2007), since it is known that $TiO_2$ crystallization and its crystallite growth are inhibited in the presence of $ZrO_2$, as shown above in the XRD results. In case of increasing calcination temperature of the pure $TiO_2$ and $0.95TiO_2$-$0.05ZrO_2$ mixed oxide, as shown in Figure 4.13, the shift of the absorption onset edges toward longer wavelength with an increase in the calcination temperature from 500 to 900 °C can be observed only in the pure $TiO_2$. As also included in Table 4.7, the band gap energy of the pure $TiO_2$ decreased from the anatase-$TiO_2$ band gap energy of 3.2 eV ($\lambda_g$ = 387 nm) at the calcination temperature of 500 °C to the rutile-$TiO_2$ band gap energy of 3.0 eV ($\lambda_g$ = 413 nm) at the calcination temperature equal or higher than 600 °C. This shift is normally due to the narrowing of the band gap energy, which results in a lower energy required for electron to be excited from the valence band to conduction band (Sreethawong *et al.*, 2009). On the other hand, the band gap energy of the $0.95TiO_2$-$0.05ZrO_2$ mixed oxide was maintained at the anatase-$TiO_2$ band gap energy, even though it was calcined at as high as 800 °C. These results confirmed that the introduction of $ZrO_2$ can inhibit the phase transformation of $TiO_2$ from the anatase to rutile phase. Moreover, with increasing calcination temperature, a decrease in the absorption band (in the wavelength between 200 and 400 nm) for the pure $TiO_2$ was greater than that for the $0.95TiO_2$-$0.05ZrO_2$ mixed oxide. This might be because of the changes in textural and structural properties. The comparative results

of UV-visible spectra of the mesoporous-assembled $0.95TiO_2$-$0.05ZrO_2$ photocatalyst calcined at 800 °C and the 0.5 wt.% Pt-loaded mesoporous-assembled $0.95TiO_2$-$0.05ZrO_2$ photocatalysts calcined at 800 °C and prepared by both the SSSG and PCD methods are shown in Figure 4.14. The band gap energies of the 0.5 wt.% Pt-loaded mesoporous-assembled $0.95TiO_2$-$0.05ZrO_2$ prepared by the SSSG and PCD methods were quite similar of approximately 3.31 eV ($\lambda_g$ ~ 375 nm) and 3.35 eV ($\lambda_g$ ~ 370 nm), respectively (Table 4.7), which were almost the same as that of Pt-unloaded sample. However, the Pt-loaded samples showed more visible light absorption ability than the unloaded sample. It can also be clearly observed that most of the $TiO_2$-$ZrO_2$ mixed oxide photocatalysts could absorb only UV light of wavelength shorter than 420 nm. Therefore, in order to confirm that Eosin Y (E.Y.) is the visible light-responding sensitizer, its UV-visible spectrum was also measured, as shown in Figure 4.15. It is clear that E.Y. could mainly absorb the visible light with the maximum absorption centered at 516 nm. This absorption feature strongly suggests that the sensitizer can be activated by the visible light for the sensitized photocatalytic hydrogen production system in this work.

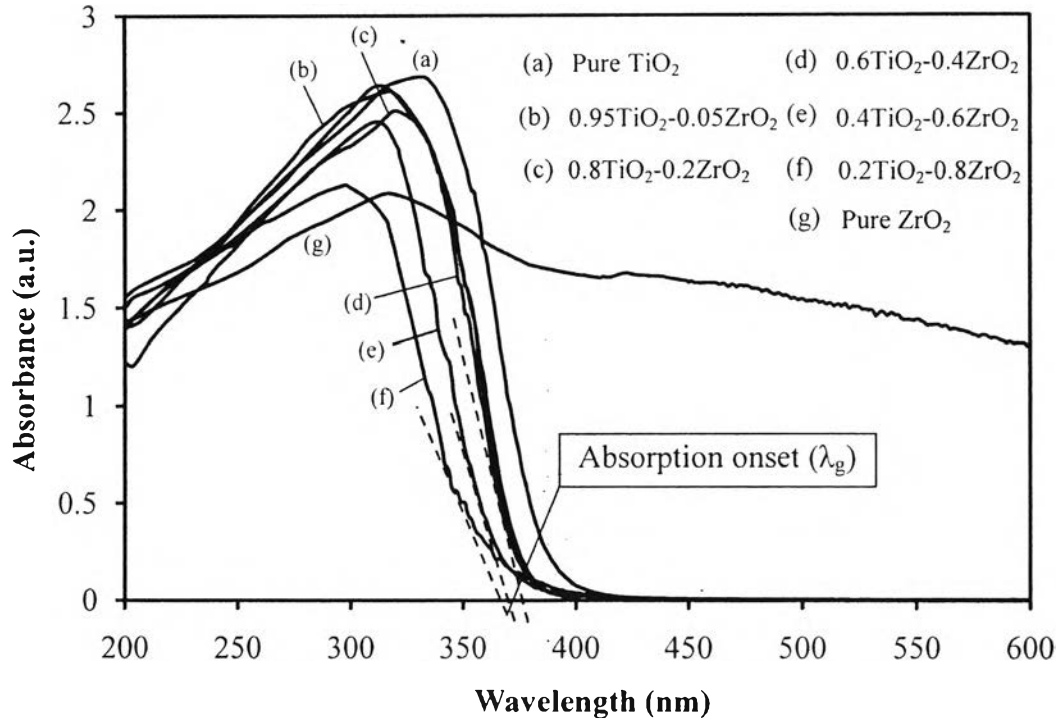


**Figure 4.12** UV-visible spectra of the mesoporous-assembled (a) pure $TiO_2$, (b)-(f) $TiO_2$-$ZrO_2$ mixed oxide, and (g) pure $ZrO_2$ photocatalysts calcined at 500 °C.

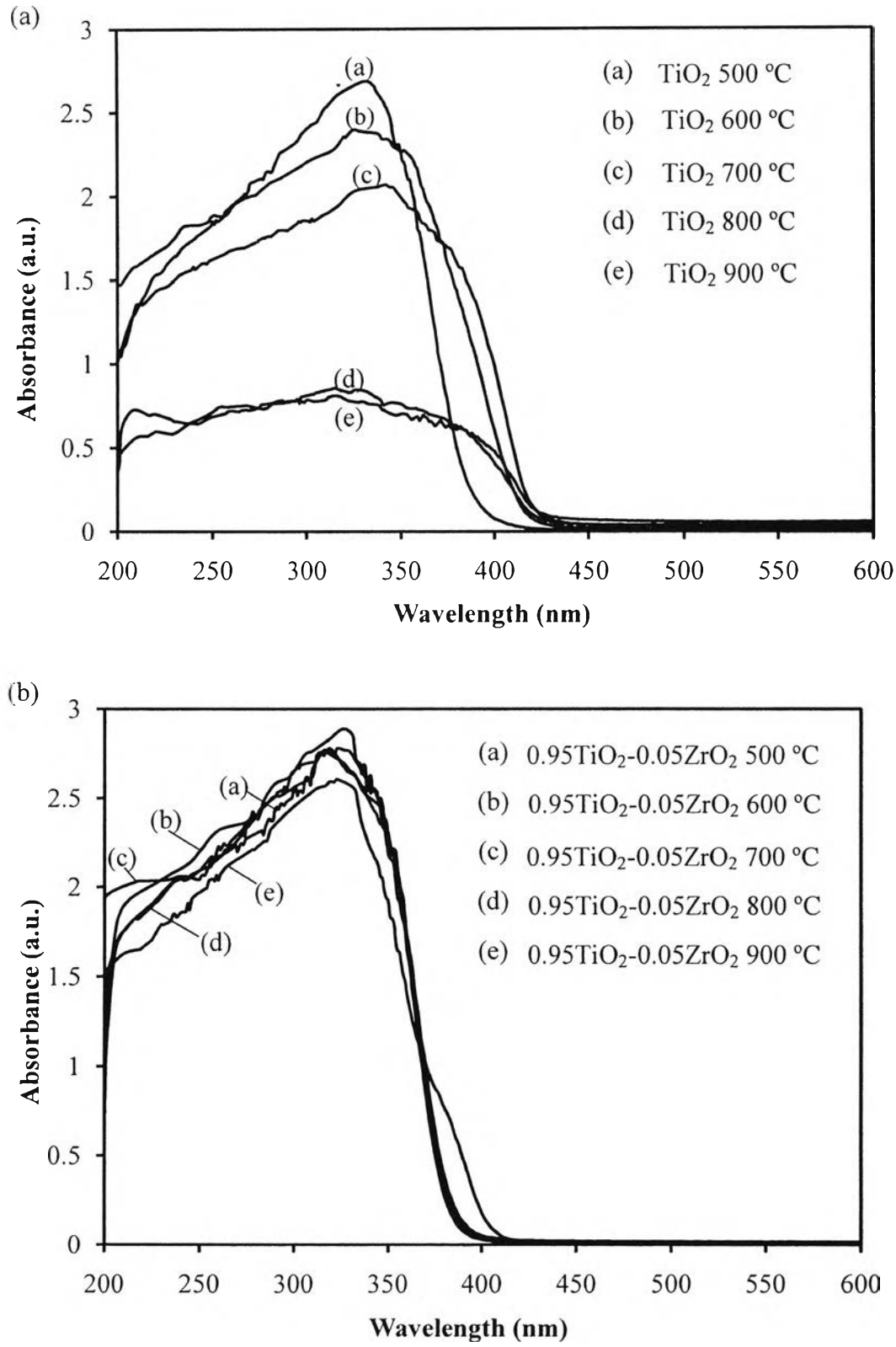


**Figure 4.13** UV-visible spectra of the mesoporous-assembled (a) pure $TiO_2$ and (b) $0.95TiO_2$-$0.05ZrO_2$ mixed oxide photocatalysts calcined at various temperatures.

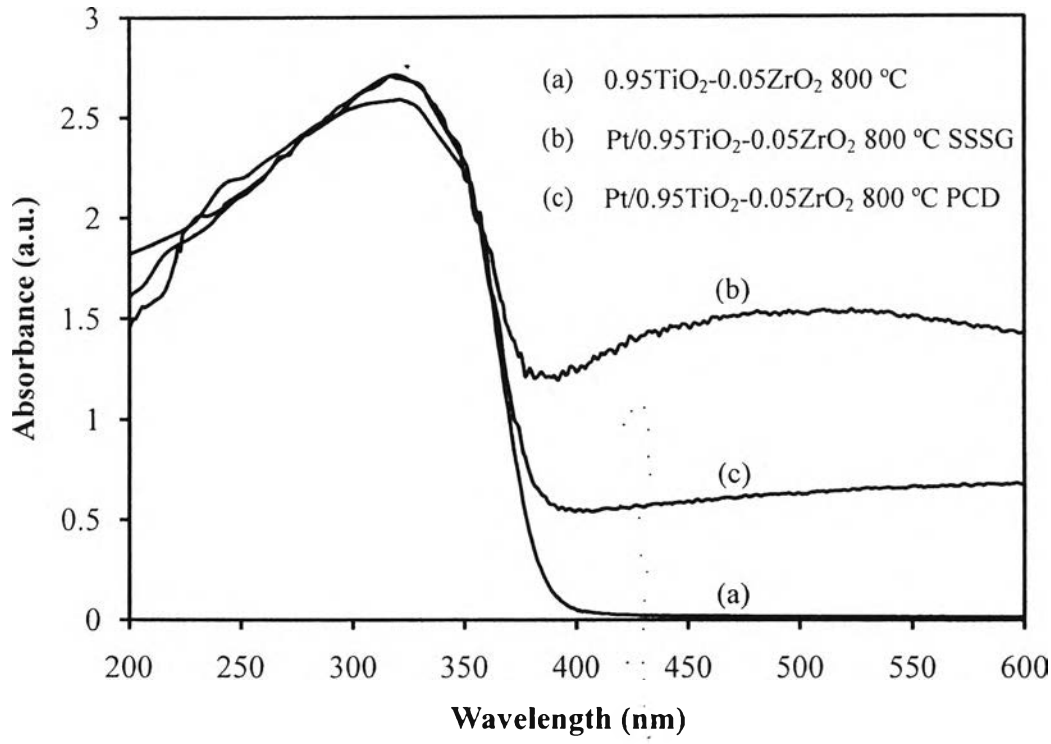


**Figure 4.14** UV-visible spectra of (a) the mesoporous-assembled $TiO_2$ photocatalyst calcined at 800 °C, and (b) and (c) the 0.5 wt.% Pt-loaded mesoporous-assembled $0.95TiO_2$-$0.05ZrO_2$ mixed oxide photocatalysts calcined at 800 °C and prepared by SSSG and PCD methods, respectively.

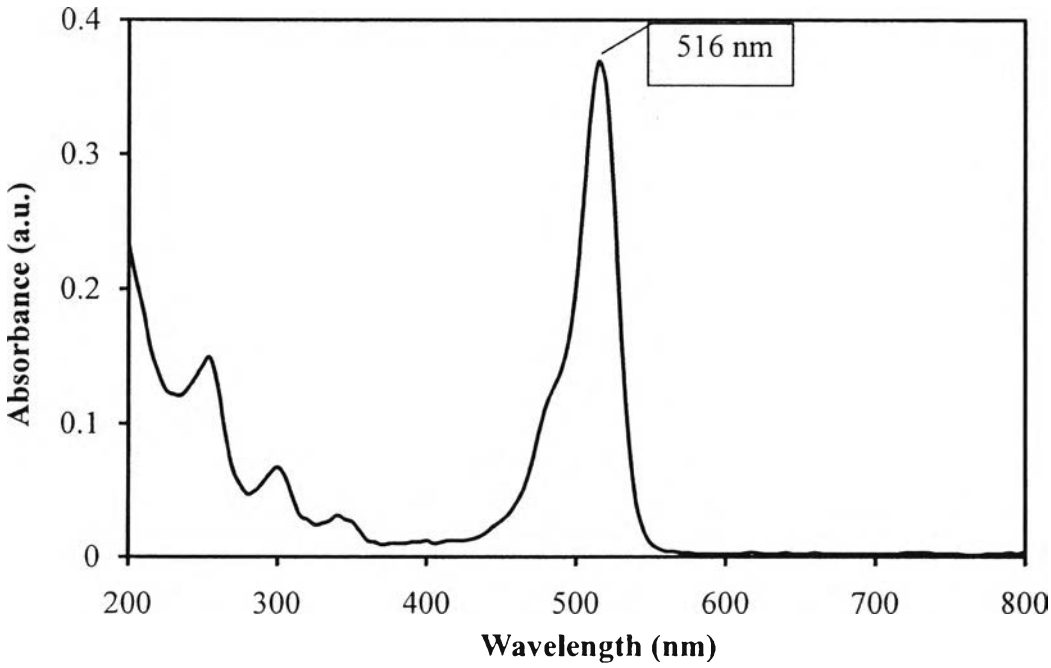


**Figure 4.15** UV-visible spectrum of Eosin Y solution.

**Table 4.7** Summary of absorption onset wavelength and band gap energy results of the synthesized mesoporous-assembled $TiO_2$-$ZrO_2$ mixed oxide photocatalysts

| Photocatalyst | Calcination temperature (°C) | Calcination time (h) | Absorption Onset wavelength, $\lambda_g$ (nm) | Band gap energy (eV) |
|---|---|---|---|---|
| Pure $TiO_2$ | 500 | 4 | 385 | 3.22 |
| | 600 | | 415 | 2.99 |
| | 700 | | 418 | 2.97 |
| | 800 | | 420 | 2.95 |
| | 900 | | 420 | 2.95 |
| $0.95TiO_2$-$0.05ZrO_2$ | 500 | 4 | 380 | 3.26 |
| | 600 | | 380 | 3.26 |
| | 700 | | 380 | 3.26 |
| | 800 | | 380 | 3.26 |
| | 900 | | 405 | 3.06 |
| $0.8TiO_2$-$0.2ZrO_2$ | 500 | 4 | 375 | 3.31 |
| $0.6TiO_2$-$0.4ZrO_2$ | | | 375 | 3.31 |
| $0.4TiO_2$-$0.6ZrO_2$ | | | 370 | 3.35 |
| $0.2TiO_2$-$0.8ZrO_2$ | | | 368 | 3.37 |
| 0.5 wt.% Pt/$0.95TiO_2$-$0.05ZrO_2$ prepared by SSSG method | 800 | 4 | 375 | 3.31 |
| 0.5 wt.% Pt/$0.95TiO_2$-$0.05ZrO_2$ prepared by PCD method | 800 | 4 | 380 | 3.26 |

4.1.5 SEM-EDX Results

The morphology of the photocatalysts was observed by the SEM analysis. Figure 4.16 shows the SEM images of the mesoporous-assembled $0.95TiO_2$-$0.05ZrO_2$ mixed oxide photocatalyst calcined at 800 °C and 0.5 wt.% Pt-loaded $0.95TiO_2$-$0.05ZrO_2$ mixed oxide photocatalyst prepared by the SSSG method and calcined at 800 °C. The images clearly reveal the presence of agglomerated clusters formed by an aggregation of several uniform-sized photocatalyst nanoparticles. Therefore, the nanoparticle aggregation plausibly led to the formation of mesoporous-assembled structure in the synthesized photocatalysts. The elemental distribution on the 0.5 wt.% Pt-loaded $0.95TiO_2$-$0.05ZrO_2$ mixed oxide photocatalysts prepared by both the SSSG and PCD methods and calcined at 800 °C were also examined by using the EDX analysis, as shown in Figures 4.17 and 4.18, respectively. The existence of dots in the elemental mappings of all investigated species (Ti, Zr, O, and Pt) show that all elements in the Pt-loaded $0.95TiO_2$-$0.05ZrO_2$ mixed oxides were well dispersed throughout the bulk photocatalysts. These results confirmed the high dispersion state of the deposited Pt particles on the mixed oxide supports prepared by both the SSSG and PCD methods.

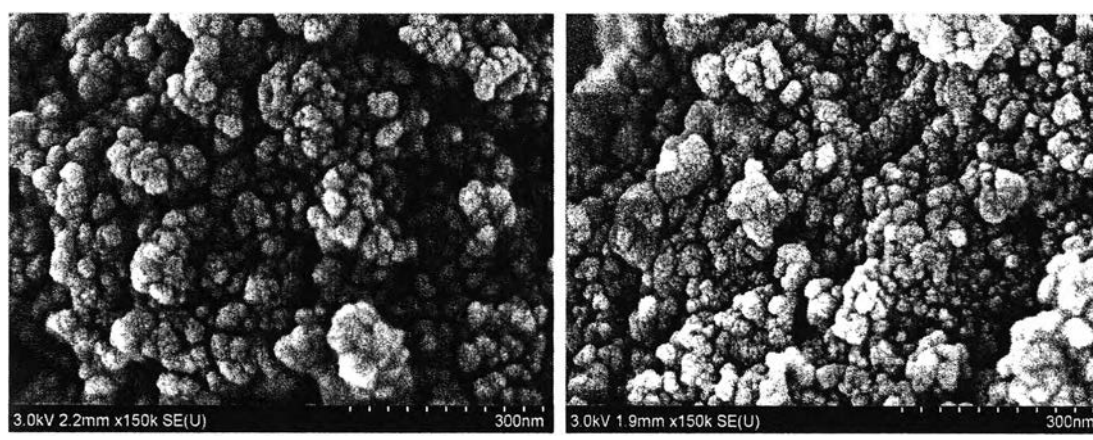


(a) (b)

**Figure 4.16** SEM images of the synthesized mesoporous-assembled photocatalysts: (a) $0.95TiO_2$-$0.05ZrO_2$ mixed oxide calcined at 800 °C and (b) 0.5 wt.% Pt-loaded $0.95TiO_2$-$0.05ZrO_2$ mixed oxide prepared by SSSG method and calcined at 800 °C.

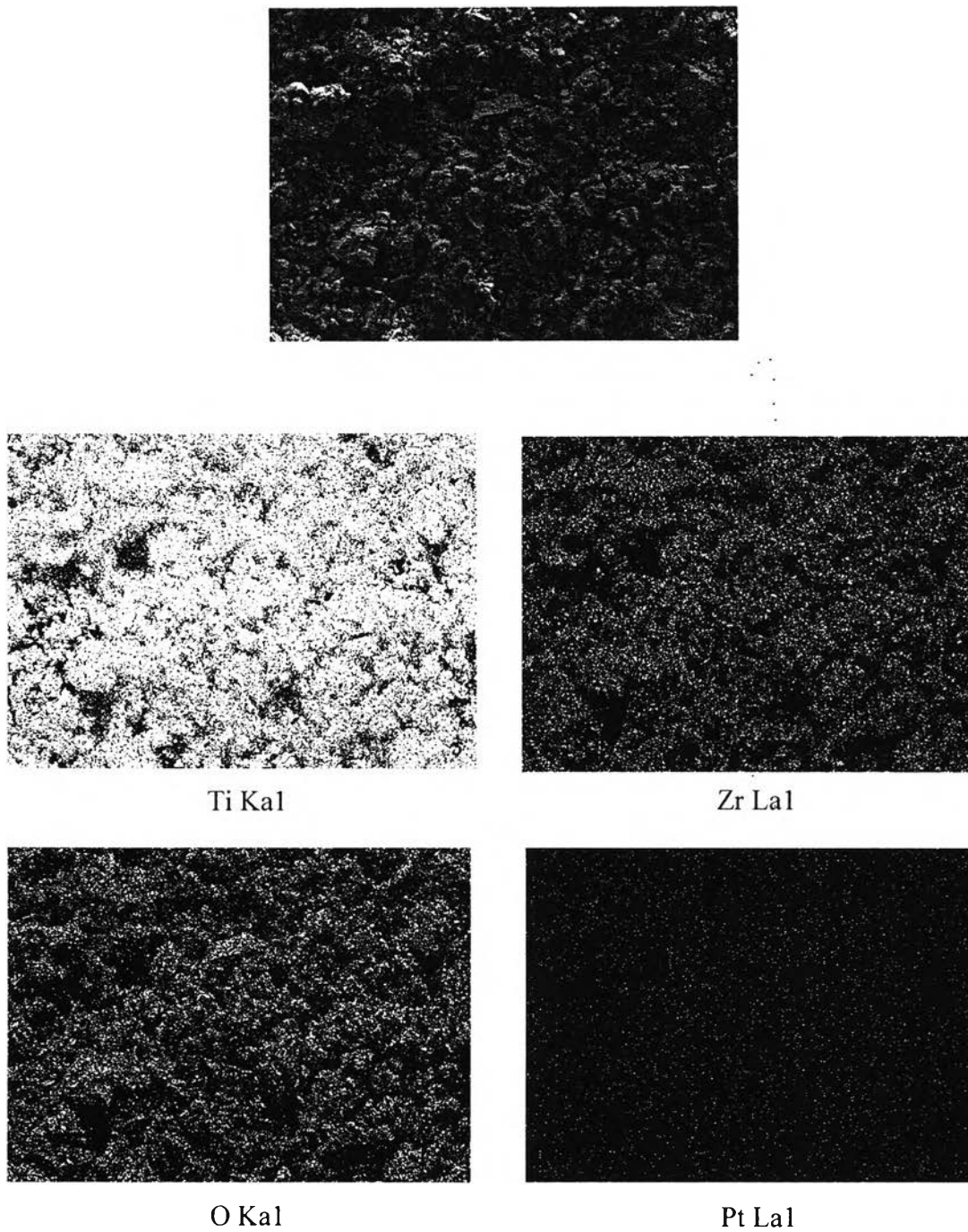


**Figure 4.17** SEM image and EDX elemental area mappings of the 0.5 wt.% Pt-loaded $0.95TiO_2$-$0.05ZrO_2$ mixed oxide photocatalyst prepared by SSSG method and calcined at 800 °C.

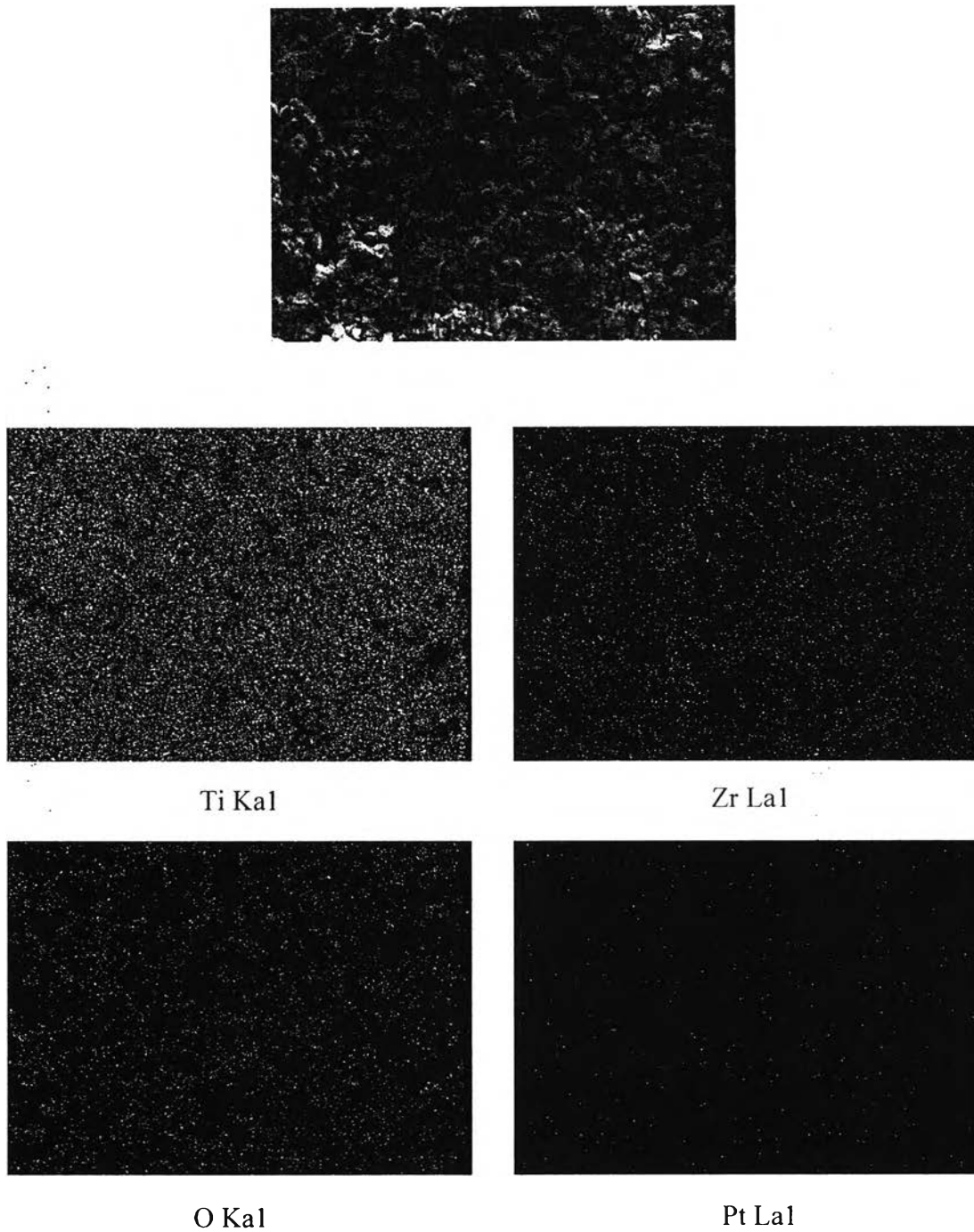


**Figure 4.18** SEM image and EDX elemental area mappings of 0.5 wt.% Pt-loaded $0.95TiO_2$-$0.05ZrO_2$ mixed oxide photocatalyst prepared by PCD method and calcined at 800 °C.

The elemental compositions of the synthesized mesoporous-assembled $0.95TiO_2$-$0.05ZrO_2$ mixed oxide photocatalysts calcined at 800 °C and without and with 0.5 wt.% Pt loading were also investigated in order to compare with the nominal elemental composition values. As shown in Table 4.8, the results reveal that all of the actual elemental compositions in the synthesized mixed oxides were found to slightly differ from the nominal values; particularly, the actual compositions of the Pt particles loaded by both the SSSG and PCD methods were almost equal to the nominal ones, indicating that there was no loss of Pt during the loading step by both methods.

**Table 4.8** Elemental composition from SEM-EDX analysis of the mesoporous-assembled $0.95TiO_2$-$0.05ZrO_2$ mixed oxide photocatalysts calcined at 800 °C for 4 h and without and with 0.5 wt.% Pt loading by SSSG and PCD methods

| Photocatalyst | Element | Weight percentage (%) | |
|---|---|---|---|
| | | Nominal composition | Actual composition |
| $0.95TiO_2$-$0.05ZrO_2$ | Ti | 55.45 | 48.06 |
| | Zr | 5.57 | 5.05 |
| | O | 38.98 | 46.89 |
| 0.5 wt.% $Pt/0.95TiO_2$-$0.05ZrO_2$ prepared by SSSG method | Ti | 55.17 | 40.07 |
| | Zr | 5.53 | 4.40 |
| | O | 38.80 | 55.02 |
| | Pt | 0.5 | 0.51 |
| 0.5 wt.% $Pt/0.95TiO_2$-$0.05ZrO_2$ prepared by PCD method | Ti | 55.17 | 47.85 |
| | Zr | 5.53 | 4.19 |
| | O | 38.80 | 47.47 |
| | Pt | 0.5 | 0.49 |

4.1.6 TEM-EDX Results

The TEM analysis was performed in order to obtain insight information about the particle sizes of Pt and $TiO_2$-$ZrO_2$ nanoparticles. Figure 4.19 shows the exemplified TEM images of the synthesized mesoporous-assembled pure $TiO_2$ calcined at 500 °C and $0.95TiO_2$-$0.05ZrO_2$ mixed oxide calcined at 500 and 800 °C. All the TEM images revealed the formation of aggregated photocatalyst nanoparticles. The average particle sizes of the photocatalysts are in the range of 10-15 nm for pure $TiO_2$ calcined at 500 °C and 8-12 nm for the $0.95TiO_2$-$0.05ZrO_2$ mixed oxide calcined at 500 °C, where the observed particle sizes are in good accordance with the crystallite sizes estimated from the XRD analysis. The smaller particle size of the mixed oxide could be attributed to an increase in the thermal stability and the resistance to sintering caused by the incorporated $ZrO_2$, as mentioned above. For the $0.95TiO_2$-$0.05ZrO_2$ mixed oxide calcined at 800 °C, which exhibited the highest photocatalytic activity among all the photocatalyst samples without Pt loading as shown later, the TEM image showed a larger particle size in the range of 10-15 nm as compared to that calcined at 500 °C. Figure 4.20 shows the TEM image and the EDX point mapping of the synthesized 0.5 wt.% Pt-loaded mesoporous-assembled $0.95TiO_2$-$0.05ZrO_2$ mixed oxide calcined at 800 °C and prepared by the SSSG and PCD methods. The Pt phase was clearly seen as dark patches on the support surface, indicating the high electron density, as confirmed by the EDX mapping. The average particle size of Pt prepared by both methods is in the range of 10-15 nm.

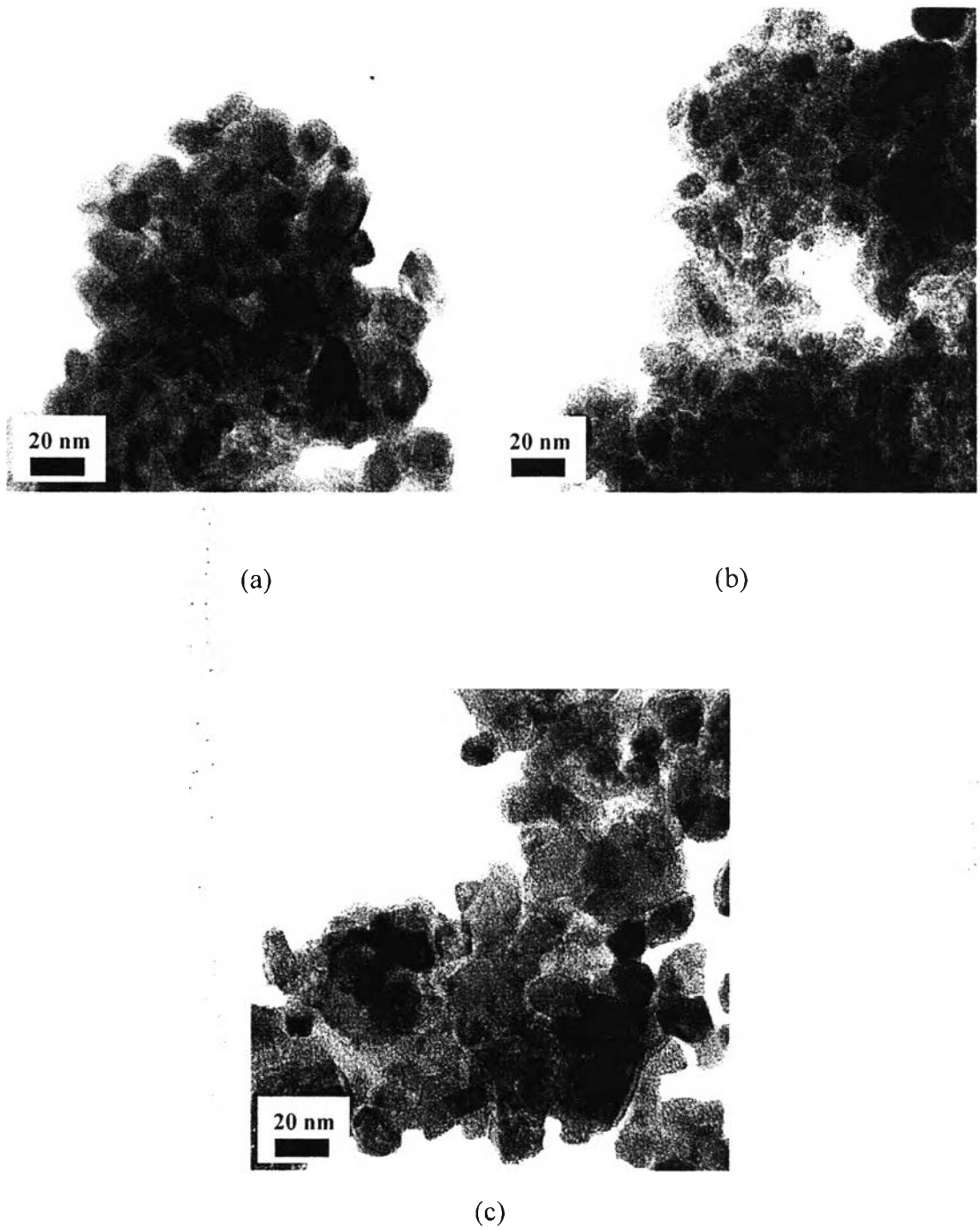


**Figure 4.19** TEM images of the synthesized mesoporous-assembled photocatalysts: (a) pure $TiO_2$ calcined at 500 °C, (b) $0.95TiO_2$-$0.05ZrO_2$ mixed oxide calcined at 500 °C, and (c) $0.95TiO_2$-$0.05ZrO_2$ mixed oxide calcined at 800 °C.

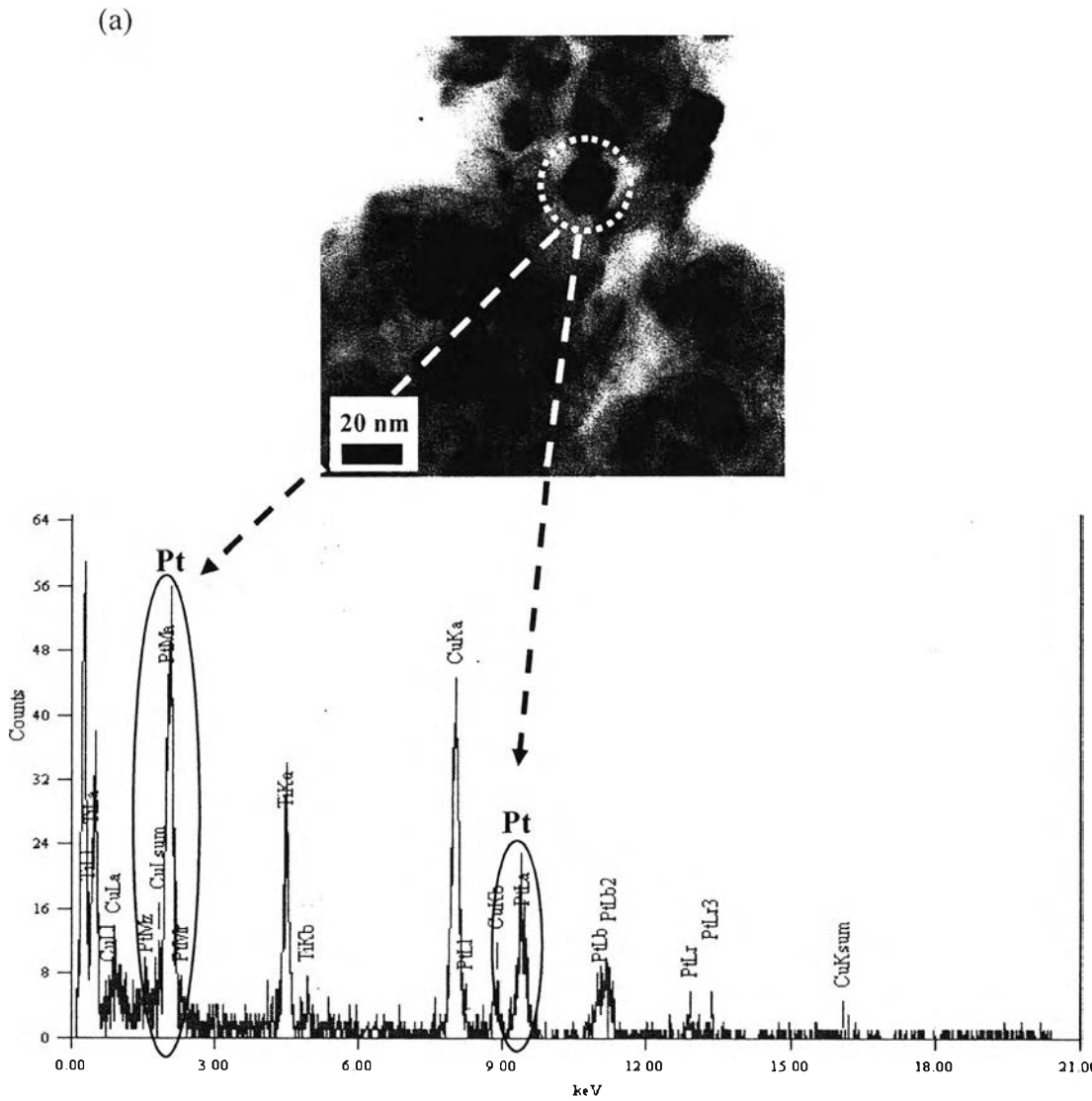


**Figure 4.20** TEM images and EDX elemental point mappings of the 0.5 wt.% Pt-loaded mesoporous-assembled $0.95TiO_2$-$0.05ZrO_2$ mixed oxide photocatalysts calcined at 800 °C and prepared by (a) SSSG and (b) PCD methods.

(b)

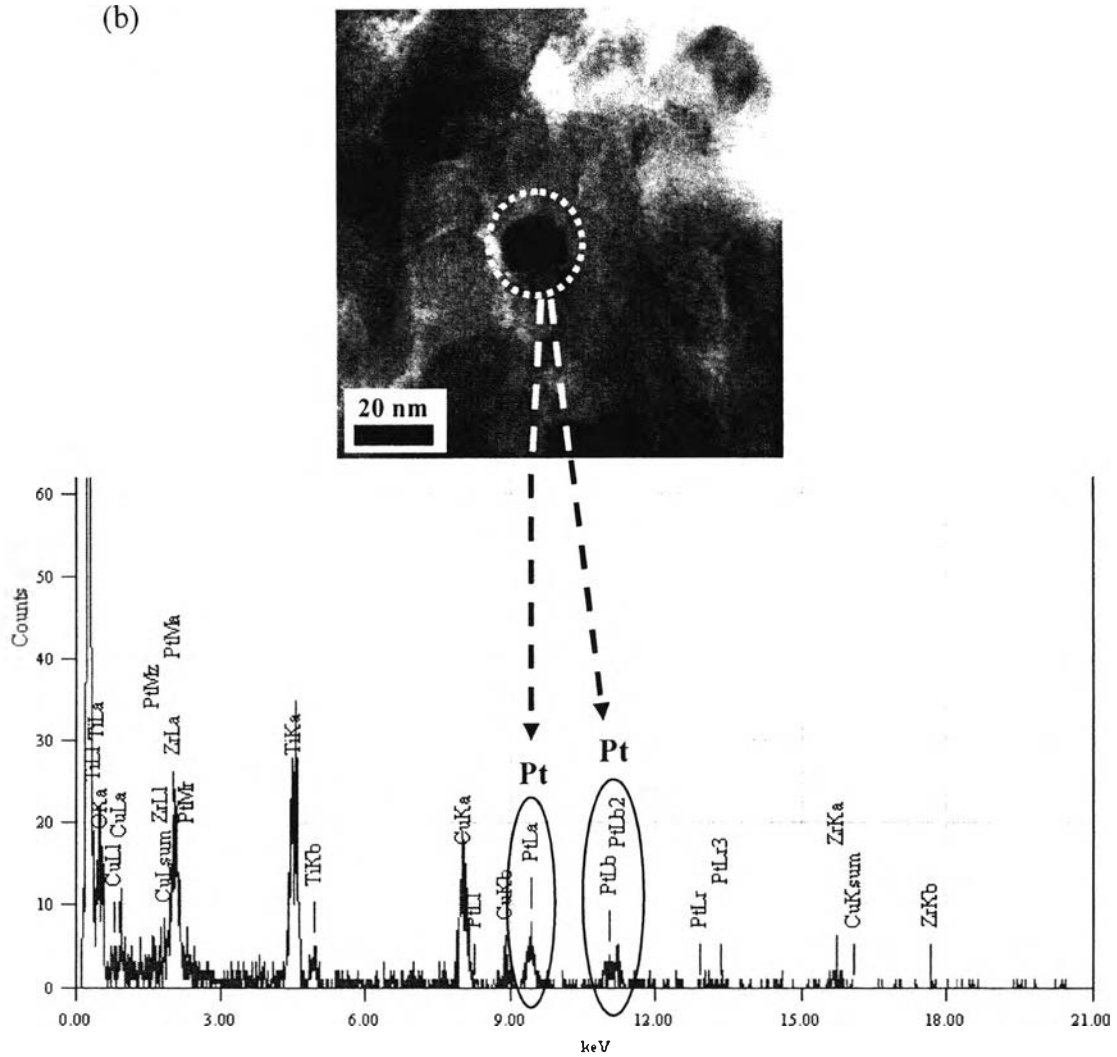


**Figure 4.20 (Continued)** TEM images and EDX elemental point mappings of the 0.5 wt.% Pt-loaded mesoporous-assembled $0.95TiO_2$-$0.05ZrO_2$ mixed oxide photocatalysts calcined at 800 °C and prepared by (a) SSSG and (b) PCD methods.

4.1.7 TPR Results

The TPR analysis was used to study the reduction property of the Pt nanoparticles loaded on the synthesized $TiO_2$-$ZrO_2$ mixed oxide photocatalysts in order to determine the Pt crystalline phase. Figure 4.21 shows the TPR profiles of the unloaded $0.95TiO_2$-$0.05ZrO_2$ mixed oxide and 0.5 wt.% Pt-loaded $0.95TiO_2$-$0.05ZrO_2$ mixed oxides prepared by the SSSG and PCD methods, all calcined at 800 °C. For the $0.95TiO_2$-$0.05ZrO_2$ mixed oxide support, a main reduction peak at temperatures higher than 400 °C was observed, and this indicates the support

reduction, mainly from $TiO_2$ to $TiO_x$ (x<2) (Wang *et at.*, 2004). For the Pt-loaded photocatalyst prepared by the SSSG method, two small reduction peaks were observed and attributed to the reduction of the platinum oxide phase ($Pt^{4+}$ to Pt), where the first one at about 100 °C can be assigned to the reduction of $Pt^{4+}$ to $Pt^{2+}$, and the second one centered at 200 °C corresponds to the reduction of $Pt^{2+}$ to metallic Pt (Pérez-Hernández *et al.*, 2005). However, the reduction peaks were small and broad, implying that only a small portion of the loaded Pt nanoparticles by the SSSG method was not in the metallic form, whereas a large portion was. Unlike the Pt-loaded photocatalyst prepared by the PCD method, there was no Pt reduction peaks observed, indicating that all of the Pt nanoparticles deposited on the photocatalyst support were in the metallic form. It was reported that photodeposited Pt particles on a $TiO_2$ surface can exist in various oxidation states, such as $Pt^{4+}$, $Pt^{2+}$, and $Pt^0$ species, and the Pt oxidation state can vary with respect to preparation conditions. Particularly, the normally used $PtCl_6^{2-}$ precursor in aqueous solution can be hydrolyzed to form $Pt(OH)_xCl_{6-x}^{2-}$ ($x$ = 1–5), and this hydrolysis process is pH-dependent (Lee *et al.*, 2005). For instance, $PtO_2$ and PtO (or $Pt(OH)_2$) were deposited in alkaline conditions through the reaction of hydrolyzed Pt complexes with VB holes (e.g. $Pt(OH)_4Cl_2^{2-} + 4h_{vb}^+ \rightarrow PtO_2 + 4H^+ + O_2 + 2Cl^-$), whereas $Pt^0$ was mainly deposited in acidic conditions in the presence of electron donors that prevent the Pt complexes from reacting with VB holes (Jin *et al.*, 1994). Since the preparation solution used for the PCD method in this work was 50 vol.% aqueous methanol solution, which was a mildy acidic solution (pH = 6.35), the deposited Pt nanoparticles on the investigated photocatalysts were accordingly in the $Pt^0$ form.

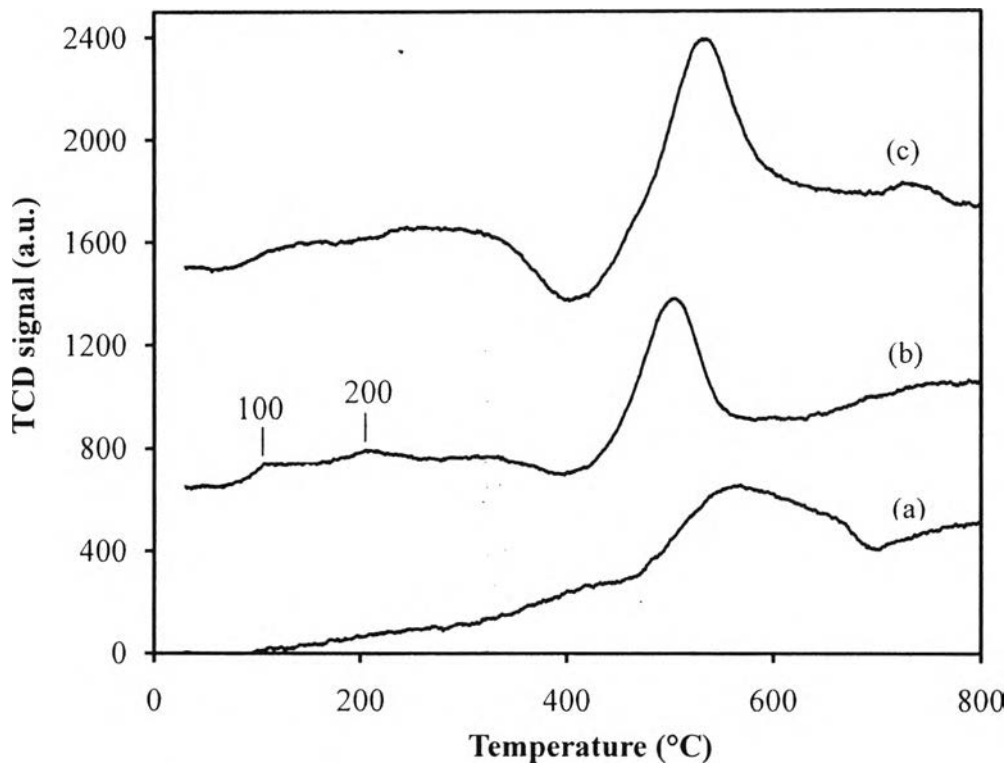


**Figure 4.21** TPR profiles of (a) the mesoporous-assembled $0.95TiO_2$-$0.05ZrO_2$ mixed oxide photocatalyst calcined at 800 °C, and (b) and (c) the 0.5 wt.% Pt-loaded mesoporous-assembled $0.95TiO_2$-$0.05ZrO_2$ mixed oxide photocatalysts calcined at 800 °C and prepared by SSSG and PCD methods, respectively.

4.1.8 $H_2$ Chemisorption Results

The Pt dispersion on the $0.95TiO_2$-$0.05ZrO_2$ mixed oxide photocatalyst was determined by using the $H_2$ chemisorption. Table 4.9 shows the Pt dispersion of the Pt-loaded $0.95TiO_2$-$0.05ZrO_2$ mixed oxide samples prepared by both the SSSG and PCD methods at various Pt loadings. For the SSSG method, the results showed that the Pt dispersion gradually increased with increasing Pt loading; however, it can be observed that all of the Pt dispersions were very low (lower than 18 %). In contrast, for the PCD method, the Pt dispersion significantly increased with increasing Pt loading from 0.3 to 0.5 wt.% and then dramatically decreased with further increasing Pt loading up to 1 wt.%. It can be comparatively seen that the PCD

method provided a higher Pt dispersion than the SSSG method at all of the investigated Pt loadings.

Table 4.10 shows the Pt dispersion of the 0.5 wt.% Pt-loaded $0.95TiO_2$-$0.05ZrO_2$ mixed oxide samples prepared by the PCD method under various UV light irradiation times and UV light intensities. In case of varying UV light irradiation time, the Pt dispersion showed the highest value of 46.1 % at the UV light irradiation time of 1 h and then slightly decreased with increasing irradiation time from 1 to 3 h; however, the Pt dispersion was observed to be almost invariant (in the range of 43-46 %) with respect to the UV light irradiation time. On the other hand, the Pt dispersion increased with increasing UV light intensity from 22 to 88 W and showed the highest value of 55.1 % at the UV light intensity of 88 W. This results imply that a higher UV intensity induced a higher Pt dispersion.

**Table 4.9** Summary of Pt dispersion results of the Pt-loaded mesoporous-assembled $0.95TiO_2$-$0.05ZrO_2$ mixed oxide photocatalysts calcined at 800 °C for 4 h and prepared by both SSSG and PCD methods

| Preparation method | Pt loading (wt.%) | Pt dispersion (%) |
|---|---|---|
| SSSG | 0.3 | 9.7 |
| | 0.5 | 12.3 |
| | 0.7 | 13.2 |
| | 1 | 17.2 |
| PCD[a] | 0.3 | 24.4 |
| | 0.5 | 45.8 |
| | 0.7 | 38.8 |
| | 1 | 19.5 |

[(a)] Prepared with UV light irradiation time of 2 h and UV light intensity of 44 W

**Table 4.10** Summary of Pt dispersion results of the synthesized 0.5 wt.% Pt-loaded mesoporous-assembled $0.95TiO_2$-$0.05ZrO_2$ mixed oxide photocatalysts calcined at 800 °C for 4 h and prepared by PCD method under various conditions

| PCD conditions | | Pt dispersion (%) |
|---|---|---|
| UV light intensity (W) | UV light irradiation time (h) | |
| 44 | 1 | 46.1 |
| | 2 | 45.8 |
| | 3 | 43.8 |
| 22 | 2 | 40.6 |
| 44 | | 45.8 |
| 88 | | 55.1 |

## 4.2 Sensitized Photocatalytic Hydrogen Production Activity

In this work, the photocatalytic activity of the synthesized mesoporous-assembled $TiO_2$-$ZrO_2$ mixed oxide photocatalysts with different $TiO_2$-to-$ZrO_2$ molar ratios calcined at various calcination temperatures without and with Pt loading was investigated for the sensitized hydrogen production from an aqueous diethanolamine (DEA) solution containing Eosin Y sensitizer (E.Y.) under visible light irradiation.

### 4.2.1 Effect of $TiO_2$-to-$ZrO_2$ Molar Ratio in Mixed Oxide Photocatalysts

In this photocatalytic reaction, 0.2 g of different types of the mesoporous-assembled $TiO_2$-$ZrO_2$ mixed oxide photocatalysts was suspended in 150 ml of 15 vol.% DEA aqueous solution (22.5 ml DEA and 127.5 ml distilled water)

containing a dissolved 0.1 mM E.Y. at room temperature, which was used as the photocatalytic reaction mixture.. The results of specific hydrogen production rate of the $TiO_2$-$ZrO_2$ mixed oxide photocatalysts with various $TiO_2$-to-$ZrO_2$ molar ratios calcined at 500 °C for 4 h are shown in Figure 4.22. It can be clearly observed that the hydrogen production rate reached a maximum value at the $TiO_2$-to-$ZrO_2$ molar ratio of 95:5. According to the surface area analysis (Table 4.2), the addition of $ZrO_2$ with an appropriate amount increased the specific surface area of the photocatalyst, consequently resulting in more available active sites on the photocatalyst surface. The obvious decrease in the photocatalytic activity at higher $ZrO_2$ contents is possibly because the $ZrO_2$ itself has a very large band gap energy greater than 5 eV (Nozik, 1978), so it cannot act as an efficient electron mediator for the sensitized hydrogen production. In addition, from the XRD results (Figure 4.6), the samples with $TiO_2$-to-$ZrO_2$ molar ratios of 40:60 and 20:80 are mainly in an amorphous phase, which is widely known to have a lower efficiency than a crystalline phase (e.g. anatase and rutile) due to an increased rate of charge recombination at the lattice defects (Ohtani *et al.*, 1997). From these results, since the mesoporous-assembled $0.95TiO_2$-$0.05ZrO_2$ mixed oxide photocatalyst provided the highest photocatalytic activity, it was selected for further experiments.

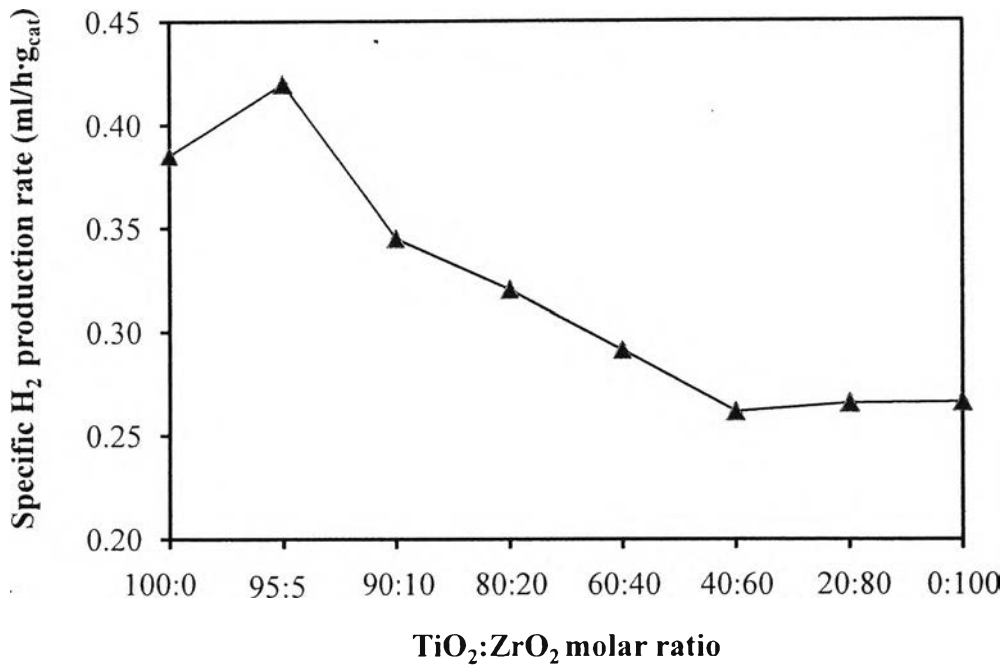


**Figure 4.22** Effect of $TiO_2$-to-$ZrO_2$ molar ratio on specific $H_2$ production rate over the mesoporous-assembled $TiO_2$-$ZrO_2$ mixed oxide photocatalysts calcined at 500 °C for 4 h (Photocatalyst, 0.2 g; total volume, 150 ml; DEA concentration, 15 vol.%; E.Y. concentration, 0.1 mM; irradiation time, 5 h).

4.2.2 Effect of Calcination Conditions

Calcination conditions significantly affect both the structural characteristics and activity of the photocatalysts. Therefore, the effects of calcination time and calcination temperature on the photocatalytic hydrogen production activity of the $0.95TiO_2$-$0.05ZrO_2$ mixed oxide photocatalyst were investigated in order to obtain the suitable conditions for the photocatalyst preparation. The effect of calcination time was first examined. Figure 4.23 shows the specific $H_2$ production rate of the $0.95TiO_2$-$0.05ZrO_2$ mixed oxide photocatalyst calcined at 500 °C for various times. The results showed that only a slight change in hydrogen production activity was observed for an increase in the calcination time from 2 to 8 h. This is in good agreement with the BET and XRD results mentioned previously that there was no significant difference in the photocatalyst characteristics by varying calcination time from 2 to 8 h. Therefore, the calcination time of 4 h was selected for further

experiments to ensure the complete crystalline structure development at each studied condition

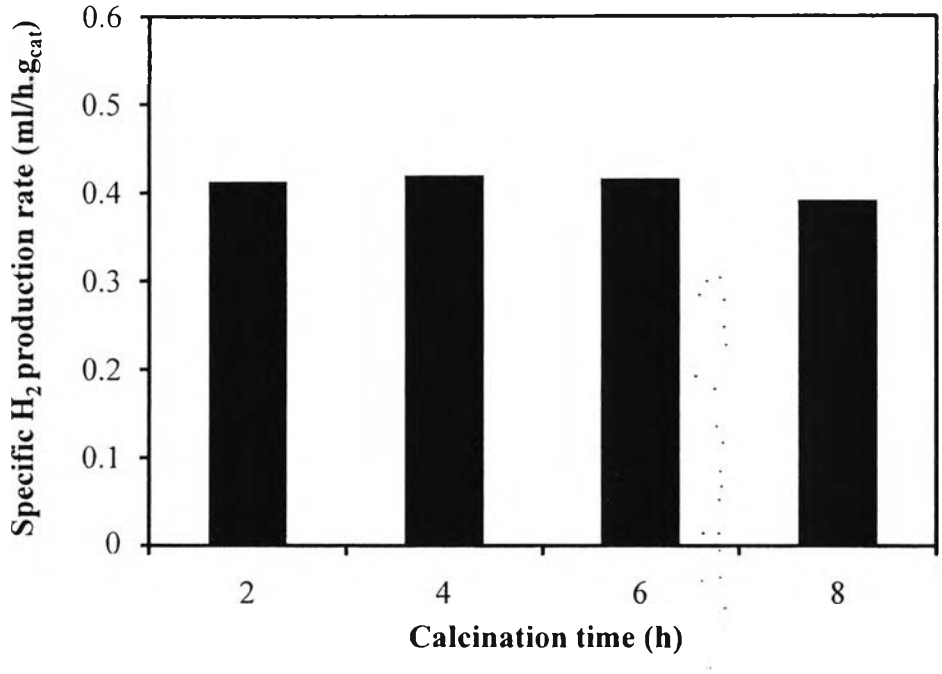


**Figure 4.23** Effect of calcination time on specific $H_2$ production rate over the mesoporous-assembled $0.95TiO_2$-$0.05ZrO_2$ mixed oxide photocatalyst calcined at 500 °C (Photocatalyst, 0.2 g; total volume, 150 ml; DEA concentration, 15 vol.%; E.Y. concentration, 0.1 mM; irradiation time, 5 h).

The effect of calcination temperature, which has a significant effect on the photocatalyst structure that can consequently lead to the change in photocatalytic hydrogen production activity, was next examined. Figure 4.24(a) shows the effect of calcination temperature on the hydrogen production activity over the mesoporous-assembled $0.95TiO_2$-$0.05ZrO_2$ mixed oxide as compared to the mesoporous-assembled pure $TiO_2$. In case of the mesoporous-assembled pure $TiO_2$, the highest photocatalytic hydrogen production was observed at the optimum calcination temperature of 500 °C at the specific $H_2$ production rate of 0.38 ml/h·$g_{cat}$. The further increase in calcination temperature resulted in a lower photocatalytic activity. This is mainly because the decrease in the photocatalyst specific surface area was observed (Table 4.2), and the photocatalyst underwent the phase

transformation from the anatase to the rutile phase (Figure 4.7(a)). It can be implied that the presence of a greater the extent of rutile phase exerts a negative effect on the photocatalytic activity. Since the rutile phase has a lower flat band potential as compared to NHE potential ($H^+/H_2$ level) than the anatase phase, this makes the rutile $TiO_2$ have a smaller driving force for the electron transfer from the excited sensitizer to its conduction band for water reduction to produce hydrogen than the anatase $TiO_2$. In contrast, the photocatalytic hydrogen production activity of the mesoporous-assembled $0.95TiO_2$-$0.05ZrO_2$ mixed oxide increased with increasing calcination temperature and reached a maximun value at the calcination temperature of 800 °C, with the specific $H_2$ production rate of 0.61 ml/h·$g_{cat}$. Since the XRD results (Figure 4.7(b)) showed that the addition of $ZrO_2$ can retard the phase transformation of the $TiO_2$ photocatalyst, the increase in the photocatalytic activity with increasing calcination temperature up to 800 °C can be explained by the growth of pure anatase crystallite size with higher crystallinity, without any rutile phase observed, leading to a smooth path for the electron transfer with less degrees of bulk defects and surface recombination sites. However, when the calcination temperature further increased to 900 °C, it was a starting point of the anatase-to-rutile phase transformation, resulting in a decreased photocatalytic activity. From a previous work (Jung *et al.*, 2002), it was also proved that the photocatalyic activity of $TiO_2$ for the decomposition of trichloroethylene (TCE) tended to increase with increasing crystallite size as long as no significant rutile phase was formed. When considering the specific $H_2$ production rate enhancement (Figure 4.24(b)), which was calculated from the Eq. (4.4):

$$\text{Specific } H_2 \text{ production rate} = \frac{\text{Rate}_{0.95TiO_2\text{-}0.05ZrO_2} - \text{Rate}_{TiO_2}}{\text{Rate}_{TiO_2}} \times 100 \qquad (4.4)$$

The results showed that the specific $H_2$ production rate enhancement of the $0.95TiO_2$-$0.05ZrO_2$ mixed oxide as compared to the pure $TiO_2$ increased with increasing calcination temperature and reached the maximum value around 94% at the calcination temperature of 800 °C.

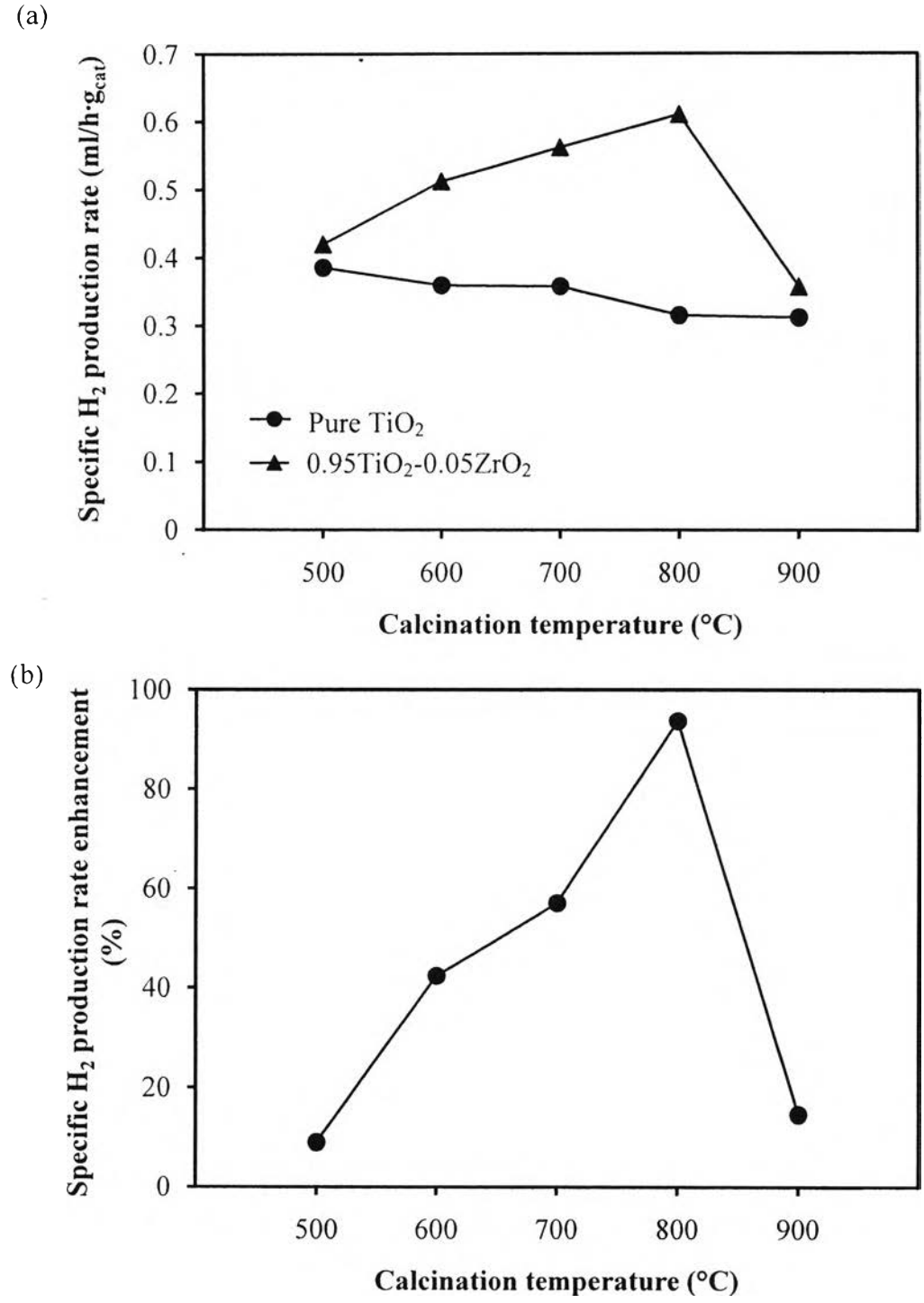


**Figure 4.24** Effect of calcination temperature on (a) specific $H_2$ production rate over the mesoporous-assembled pure $TiO_2$ and 0.95$TiO_2$-0.05$ZrO_2$ photocatalysts (b) specific $H_2$ production rate enhancement (Photocatalyst, 0.2 g; total volume, 150 ml; DEA concentration, 15 vol.%; E.Y. concentration, 0.1 mM; irradiation time, 5 h).

4.2.3 Effect of Pt Loading

Noble metals are normally used to load on a photocatalyst surface to solve the problem of the charge carrier recombination that can result in the low photocatalytic activity. The most active metal for photocatalytic enhancement is Pt, which can produce the highest Schottky barrier among the metals that facilitate the electron capture for further photocatalytic reaction (Vorontsov *et al.*, 1999). Figure 4.25 shows the results of specific hydrogen production rate as a function of Pt loading of the Pt-loaded mesoporous-assembled $0.95TiO_2$-$0.05ZrO_2$ photocatalysts prepared by both the SSSG and PCD methods. Similar trends of the photocatalytic activity were observed for the photocatalysts prepared by both methods with various Pt loadings; the specific hydrogen production rate increased with increasing Pt loading and reached an optimum value before decreasing when the Pt loading was higher than 0.5 wt.%. Therefore, these results imply that the Pt loading of 0.5 wt.% was the most suitable Pt content for the investigated photocatalysts. Since the surface areas and crystallite sizes of both the photocatalysts remained almost unchanged with varying Pt loading, as shown in Tables 4.3 and 4.6, the increase in the hydrogen production rate with increasing Pt loading from 0 to 0.5 wt.% can be explained in that the loading of Pt can enhance the photocatalytic reaction by promoting the charge separation and serving as the active hydrogen production sites. However, when the Pt loading exceeded a critical limit (i.e. an optimum loading of 0.5 wt.%) where the agglomeration process takes place, some of them inevitably act as the electron-oxidized sensitizer recombination centers that can negatively lead to a decrease in the photocatalytic activity (Zou *et al.*, 2007). Therefore, there is an optimum amount of Pt loading for the maximum hydrogen production activity. It can be clearly seen that under the studied range of Pt loading, the Pt-loaded photocatalyst prepared by the PCD method always exhibited a higher hydrogen production rate than that prepared by the SSSG method. For the Pt-loaded photocatalyst prepared by the SSSG method, the maximum hydrogen production rate was 1.42 $ml/h \cdot g_{cat}$ at the optimum Pt loading, while the hydrogen production rate of the Pt-loaded photocatalyst prepared by the PCD method reached the maximum value of 2.37 $ml/h \cdot g_{cat}$, being almost two times of that of the SSSG-prepared photocatalyst. These results point out that the more efficient charge separation at the interface of Pt

nanoparticles and $TiO_2$-$ZrO_2$ mixed oxide support was obtained in the PCD-prepared photocatalyst. These can be possibly explained by the TPR results (Figure 4.21) that the loaded Pt nanoparticles in the SSSG-prepared photocatalysts were partly in the oxide form, whereas these in the PCD-prepared photocatalysts were all in the metallic form. As there is a previous study reporting that a $TiO_2$ loaded with oxidized Pt species ($Pt_{ox}/TiO_2$) was less reactive than that loaded with metallic Pt ($Pt^0/TiO_2$) as ascribed to the negative role of the $Pt_{ox}$ species as a recombination center (Lee *et al.*, 2005), it is therefore generally accepted that metallic Pt ($Pt^0$) is its most favorable oxidation state for the photocatalytic reaction. Moreover, the Pt-loaded photocatalyst prepared by the SSSG method may lose some photocatalytic efficiency due to a less number of surface-exposed Pt nanoparticles since some of them may be possibly buried in the bulk photocatalyst during the sol-gel procedure, which can be considered inactive for the photocatalytic reaction. In addition, from the TPR results (Table 4.9), the low Pt dispersions (lower than 18 %) of the SSSG-prepared photocatalysts hardly affected the photocatalytic activity, whereas those of the PCD-prepared photocatalysts corresponded very well to the photocatalytic activity, exhibiting a maximum hydrogen production rate at 0.5 wt.%, at which the highest Pt dispersion (45.8%) was observed.

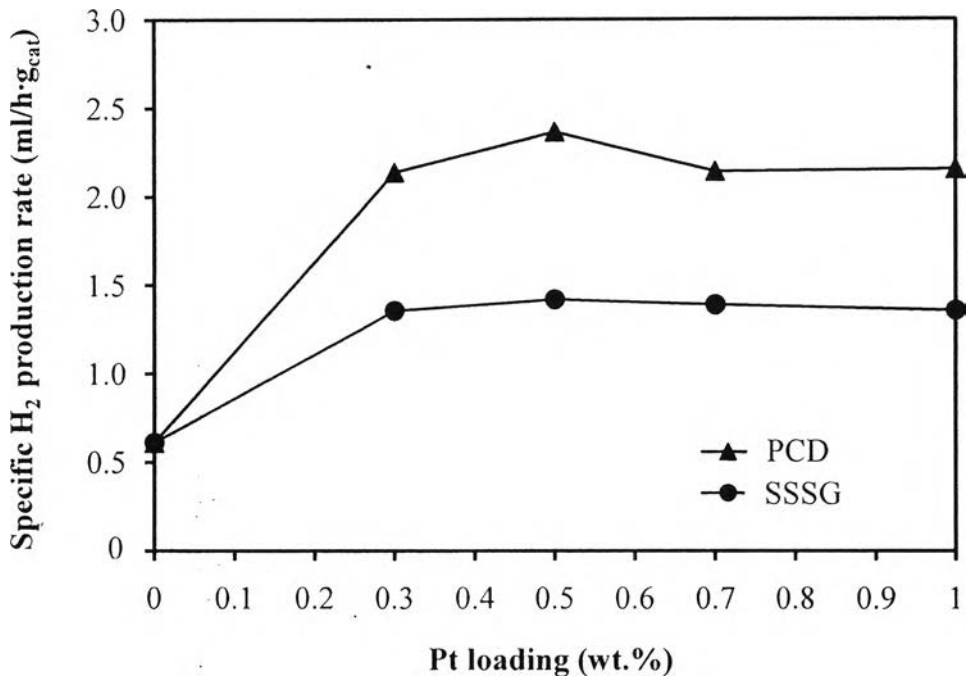


**Figure 4.25** Effect of Pt loading on specific $H_2$ production rate over the mesoporous-assembled $0.95TiO_2$-$0.05ZrO_2$ photocatalysts calcined at 800 °C for 4 h and prepared by SSSG and PCD methods (Photocatalyst, 0.2 g; total volume, 150 ml; DEA concentration, 15 vol.%; E.Y. concentration, 0.1 mM; irradiation time, 5 h).

4.2.4 Effect of Photochemical Deposition Conditions

As clearly seen from the above results that the 0.5 wt.% Pt-loaded $0.95TiO_2$-$0.05ZrO_2$ mixed oxide photocatalysts prepared by the PCD method provided a higher hydrogen production rate than those prepared by the SSSG method, the conditions used in the PCD preparation were therefore further investigated in order to obtain the most suitable conditions that provided the highest hydrogen production activity. Figure 4.26 shows the hydrogen production activity of the 0.5 wt.% Pt-loaded $0.95TiO_2$-$0.05ZrO_2$ photocatalysts prepared by the PCD method under UV light irradiation times. The results showed that there were no significant differences in the specific $H_2$ production rate by varying UV light irradiation time; however, the UV light irradiation time of 2 h was selected for further investigation on the effect of UV light intensity in order to sufficiently provide enough deposition time for Pt nanoparticles under any studied conditions. In contrast, the UV light intensity was found to have a more significant impact on the photocatalytic hydrogen

production activity than the UV light irradiation time. The results shown in Figure 4.27 revealed that the UV light intensity of 44 W provided the highest specific $H_2$ production rate. A lower or higher intensity (22 or 88 W) provided slightly lower specific $H_2$ production rate than 44 W. Since the textural and structural properties of the Pt-loaded photocatalysts remained almost unchanged (Table 4.4 and Figures 4.10 and 4.11), the Pt dispersion should be rather considered. From the Pt dispersion results (Table 4.10), as the Pt dispersion was found to be almost invariant with respect to the UV light irradiation time, the specific $H_2$ production rate became nearly constant, as expected. In contrast, in the case of varying UV light intensity, the Pt dispersion of about 45.8% at the UV light intensity of 44 W provided the highest specific $H_2$ production rate, indicating that a higher Pt dispersion led to a higher number of active sites on the photocatalyst surface. However, a too high Pt dispersion of about 55.1 % at the UV light intensity of 88 W was found to be unfavorable for the $H_2$ production, possibly because the Pt nanoparticles with a too high Pt dispersion induce a more probability of surface charge recombination, resulting in an observed lower photocatalytic activity.

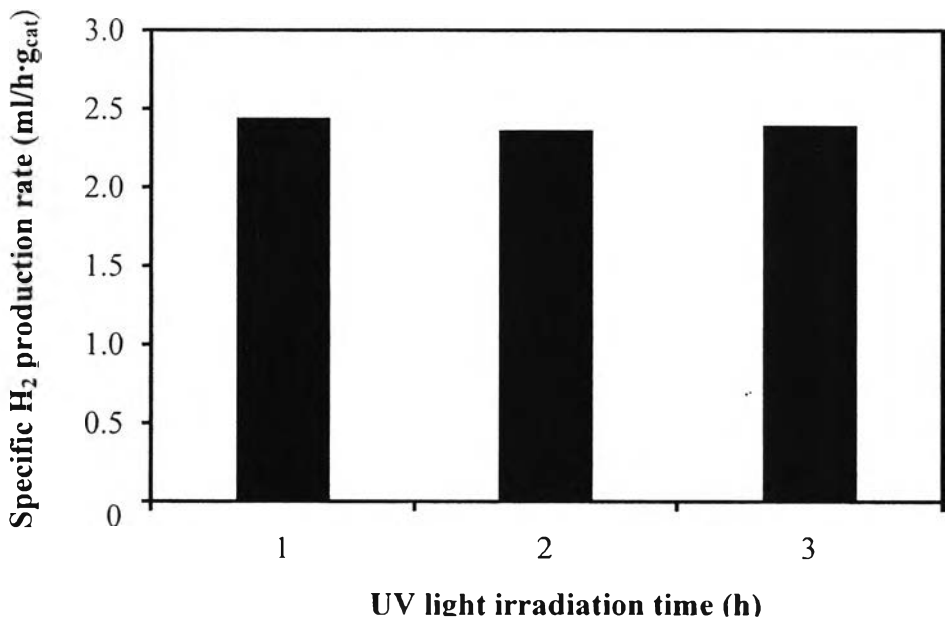


**Figure 4.26** Effect of UV light irradiation time at the UV light intensity of 44 W on specific $H_2$ production rate over the 0.5 wt.% Pt-loaded $0.95TiO_2$-$0.05ZrO_2$ photocatalyst prepared by PCD method (Photocatalyst, 0.2 g; total volume, 150 ml; DEA concentration, 15 vol.%; E.Y. concentration, 0.1 mM; irradiation time, 5 h).

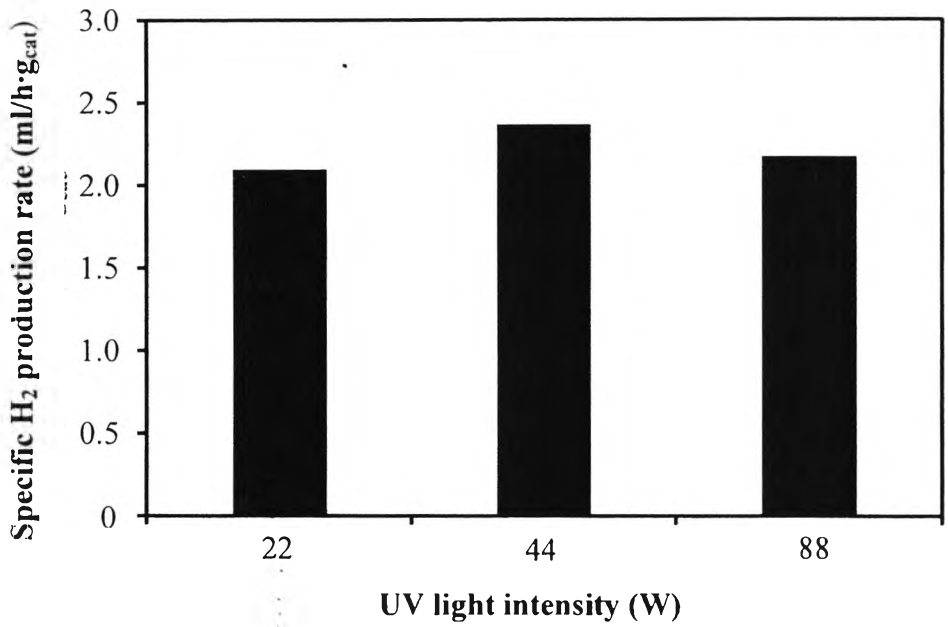


**Figure 4.27** Effect of UV light intensity at the UV light irradiation time of 2 h on specific $H_2$ production rate over the 0.5 wt.% Pt-loaded $0.95TiO_2$-$0.05ZrO_2$ photocatalyst prepared by PCD method (Photocatalyst, 0.2 g; total volume, 150 ml; DEA concentration, 15 vol.%; E.Y. concentration, 0.1 mM; irradiation time, 5 h).

4.2.5 Photocatalyst Durability

In order to study the photocatalyst durability in the sensitized photocatalytic hydrogen production system, the sensitized 0.5 wt.% Pt-loaded $0.95TiO_2$-$0.05ZrO_2$ photocatalyst prepared by the PCD method, which provided the highest hydrogen production activity, was used in this test. The photocatalytic activity of the photocatalyst was studied for 3 consecutive runs. After finishing 5 h irradiation of the first run, the photocatalyst powder was recovered. Before the next run, the recovered photocatalyst was either not heat-treated or heat-treated at 800 ° for 1 h. Figure 4.28 shows that the photocatalytic hydrogen production rates of the photocatalyst without heat treatment after recovery for the 3 consecutive runs were 2.37, 2.01, and 1.67 ml/h·$g_{cat}$, respectively. From the results, it can be seen that the hydrogen production rate gradually decreased after the first run. A decrease in the hydrogen production rate might possibly originate from that there were some reaction mixture species, such as inactive E.Y. and DEA, strongly adsorbing on the

photocatalyst surface, and this make it gradually deactivated. Hypothetically, in order to remove the adsorbed species to regenerate the photocatalyst, the recovered photocatalyst should be heat-treated. In this experiment, the photocatalyst recovered from the first run was calcined for 1 h at 800 °C (the temperature used to stabilize the photocatalyst structure during the calcination step), and then was used in the second run. The result from the second run showed that the hydrogen production rate still decreased from the first run and was even lower than that from the second run of the recovered photocatalyst without the heat treatment. The lower photocatalytic activity may be due to the growth of Pt nanoparticles during the heat treatment at 800 °C. Therefore, an effective way to maintain the photocatalytic activity for several consecutive runs, or long-period irradiation time, is needed to be further investigated.

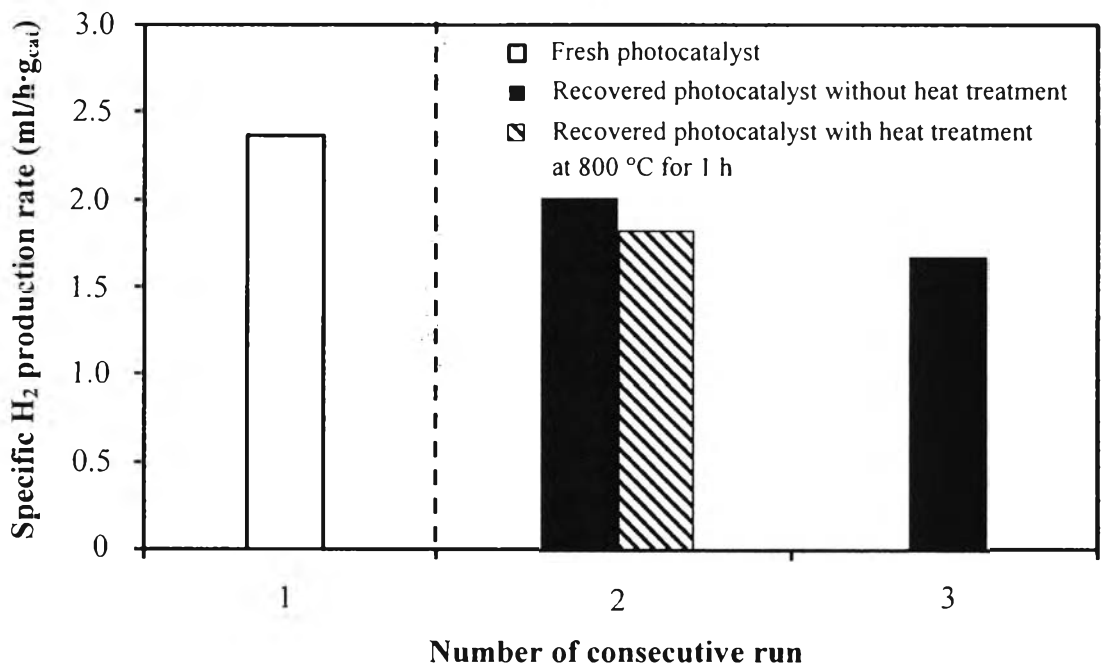


**Figure 4.28** Durability of the 0.5 wt.% Pt-loaded $0.95TiO_2$-$0.05ZrO_2$ photocatalyst prepared by PCD method calcined at 800 °C in the sensitized hydrogen production system for 3 consecutive runs (Photocatalyst, 0.2 g; total volume, 150 ml; DEA concentration, 15 vol.%; E.Y. concentration, 0.1 mM; irradiation time, 5 h).